Responses to Referee #1

The paper describes a monitoring study of trace gases at a suburban site close to the airport in Hong Kong. A comparison is made of ozone concentrations over a ten-year period via detailed analysis of three periods, coupled with master chemical mechanism/box model calculations to facilitate interpretation. This analysis is coupled with a source apportionment analysis for VOCs and with discussion of policy changes in the area. The study is one of a sequence of detailed papers that have investigated air quality, and especially ozone production, in this area, especially in relation to air quality policy. This paper adds to that corpus of knowledge and understanding and should be published. The authors should consider the following points:

We highly appreciate the reviewer for the comments and suggestions. More detailed information is supplemented in the revised manuscript according to the reviewer's concerns.

1. The introduction gives references to the large series of investigations of which this paper is the latest. It is important to understand what these papers have contributed to our understanding of air quality in Hong Kong, and information is provided, but it is quite difficult to appreciate fully. It would be helpful if a table was provided, listing the main contributions (not all need be included and there are some overlaps) of these papers: target pollutant, nature of the monitoring, main conclusions.

Thank you for this good comment. Table S1, as suggested, is provided in the revised manuscript supplementary, which lists the contributions of previous papers to the understanding on O_3 pollution in Hong Kong.

Revisions have been made as follows.

Overall, the previous studies have greatly enhanced our understanding on O_3 pollution in Hong Kong, and details about the studies can be referred to in Table S1.

For details, please refer to lines 87-89, page 4 and Table S1.

2. The main aim of the paper is to investigate the changes in ozone through measurement of the major inorganic species, including ozone, and a wide range of VOCs, at a single site. The observations are supported and interpreted using a box model based on the master chemical mechanism. There are several issues that warrant further discussion than they are given in the text, and some clarifications:

i) The site (Tung Chung, TC) is close to a highway serving the airport which is only 3 km away. The mean NO and NO_2 concentrations are not too high, but the maximum values are. It is commented that one reason for low [O3] could be titration by NO. An analysis of the degree of titration would be helpful.

Thank you for the good suggestion.

Located in a newly-developed town in western Hong Kong, TC site is expected to be influenced by local vehicle emissions and emissions from the nearby airport highway (Wang et al., 2018b). In TC, the daytime NO peaks usually occur at around 8:00 and 19:00 LT, attributable to the vehicular emissions in the morning and evening rush hours. Therefore, in the early morning (7:00 – 8:00 LT), the nocturnal steady-state O_3 is titrated by the freshly emitted NO, forming a trough in the diurnal cycle of O_3. Here, the decrease of O_3 in the early morning is employed to represent the degree of NO titration to O_3, ΔO_3-1 in Figure S1 taking the diurnal

cycle of O_3 in 2007 as an example. Correspondingly, ΔO_3-2, the difference between the maximum O_3 in the afternoon and the minimum O_3 in the morning, reflects the photochemical production of O_3 in daytime. According to Figure S1, the O_3 titrated by NO (ΔO_3-1) was 9.2 ±2.1, 9.8 ±2.7 and 6.8 ±2.7 ppbv, equivalent to 29.9 ±8.8%, 26.7 ±12.7% and 32.5 ±16.6% of the photochemically formed O_3 (ΔO_3-2) in 2007, 2013 and 2016, respectively.

The discussions on the degree of titration have been added into the revised manuscript.

It was expected that O_3 at TC would be significantly influenced by NO emitted from the aforementioned sources. As shown in Figure S1, the O_3 titrated by NO (ΔO_3-1) was equivalent to 29.9 ±8.8%, 26.7 ±12.7% and 32.5 ±16.6% of the photochemically formed O_3 (ΔO_3-2) in the 2007, 2013 and 2016 sampling campaigns, respectively, confirming the importance of NO titration in modulating O_3 at the site.

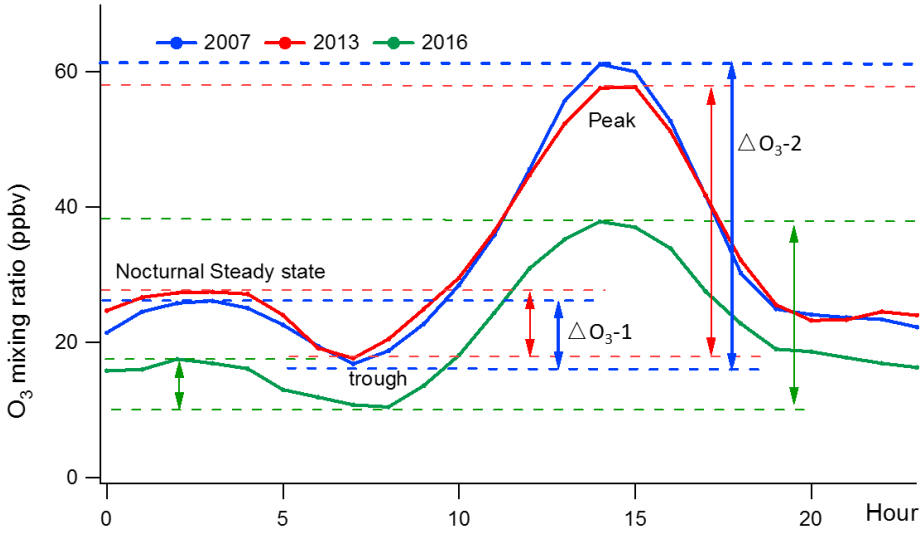

Figure S1. Average diurnal cycles of O_3 in the 2007, 2013 and 2016 sampling campaigns. ΔO_3-1: O_3 decrease in the early morning driven by NO titration; ΔO_3-2: photochemically formed O_3 in the daytime (diurnal cycle of O_3 in 2007 as an example).

For details, please refer to lines 140-145, page 6 and Figure S1.

ii) The paper is based on analysis of three periods covering 2007-2016. There can be significant year to year variations resulting, for example, form meteorological rather than AQ policies. Figure 2 shows that long term trends in hourly ozone at TC and shows that decreases have, on average, occurred since 2013. The figure is very difficult to interpret, though, since it shows log[O_3]. The low concentrations, presumably at night, are of little interest. It would be much easier to understand what is happening if this plot were linear in [O_3].

Thanks for this good comment and the suggestion. To make the variation trends of O_3 clearer, we re-plotted Figure 2 with the linear [O_3].

According to the updated Figure 2, O_3 was identified to be increased from 2007 to 2013, which however decreased between 2013 and 2017, consistent with the previous results. The patterns were discernible from both the continuous measurements of O_3 and the O_3 observed in the three VOC sampling periods (Lines 323-348, pages 14-15 in the manuscript). It cannot be denied that the meteorological conditions played roles in influencing the O_3 trends. For example, the lower O_3 in the autumn of 2016 could be partially explained by the less frequent tropical cyclones and continental anticyclones, as discussed in lines 375-388, pages 16-17. However, the simulation of in situ photochemistry in previous studies (Xue et al., 2014a; Wang et al., 2017a; Lyu et al., 2017b) and this paper also indicated the effects of air quality policies on O_3 variations in Hong Kong. In addition, a recent study (Li et al., 2019) published in PNAS (Proceedings of the National Academy of Sciences of the United States of America) demonstrated the significant effects of artificial interventions on O_3 pollution in China with the filtration of meteorological impacts. The statistically unchanged O_3 residues (differences between observed O_3 and O_3 driven by meteorological conditions) during 2013 – 2017 in most

areas of PRD corroborated our finding that the contribution of regional transport to O_3 in Hong Kong stopped increasing since 2013. This reinforces our confidence in the conclusions of this study.

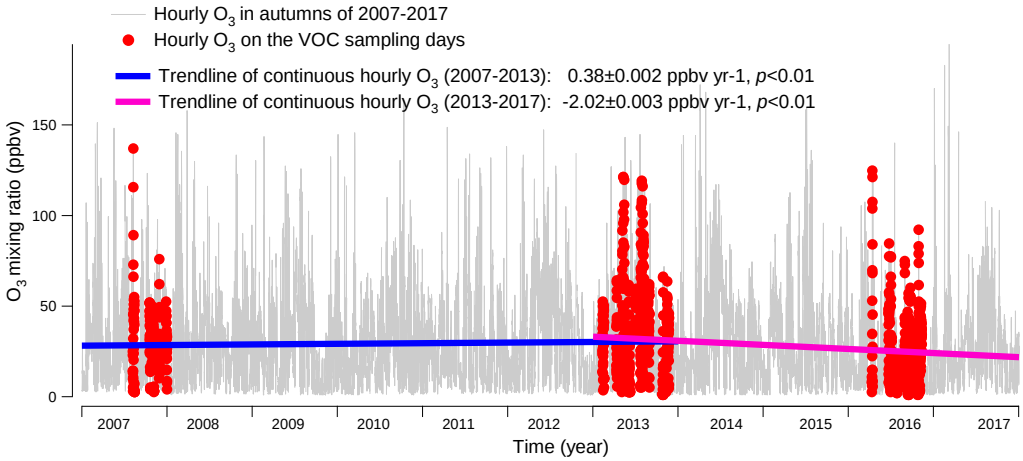

Figure 2. Long-term trends of the observed O_3 at TC from 2007 to 2017. Hourly O_3 values on the VOC sampling days in the autumns of 2007, 2013 and 2016 are marked in red. The hourly variation rates of O_3 are converted to yearly rates in periods of 2007 – 2013 and 2013 – 2017.

For details, please refer to Figure 2.

iii) Some further discussion of the locally produced and regionally transported ozone (p5 line 109) would be helpful. The wind speeds are generally quite low, so the distances the precursors and ozone itself are transported is not large. How significant is precursor transport? Are the sources greater in some directions for the longer-lived precursors? How significant is this? The assertion that the regionally transported emissions can be determined by difference as asserted on p5 needs some moderation-the chemistry isn't linear and the simulations aren't 100% accurate, as demonstrated by some apparently negative regional sources.

We highly appreciate the thoughtful comments and suggestion.

The winds were indeed low at the sampling site, which were likely weakened by the surrounding buildings. In fact, the wind speeds monitored at the Hong Kong International Airport which was ~3 km to the north of the site were much higher (>4 m/s, see Table S6 for details), indicating that air pollutants could be transported from PRD to the area where the site located. As shown in Figure S2, some O_3 precursors, including both the longer-lived species (*e.g.* CO, ethyne, ethane and propane) and shorter-lived species (*e.g.* toluene) exhibited higher concentrations under some wind sectors (such as the northwest winds), relative to the average concentrations under the light winds (wind speeds < 2m/s). Therefore, regional transport at least made some contributions to the O_3 precursors at the sampling site. Considering that the concentrations of air pollutants measured under light winds represented the local emissions, regional transport elevated the concentrations of CO, ethyne, ethane, propane and toluene by up to 11.3%, 48.0%, 42.5%, 53.5% and 138.5%, respectively.

The regionally-transported O_3 precursors made some contributions to the in-situ O_3 production. Therefore, the locally-produced O_3 were somewhat overestimated by assigning the simulated O_3 as the locally produced O_3. In addition, the nonlinear chemistry and model uncertainty raised by the reviewer also caused some uncertainties in the locally-produced and regionally-transported O_3 determined in this study, which are discussed in Text S1.

However, we may clarify that the negative values of regionally-transported O_3 were not necessary to be only caused by the uncertainties, but also indicative of the quick dispersion and dilution of O_3 by the south winds from the relatively clean South China Sea in most cases.

Discussions have been added in the revised manuscript.

With the aid of a photochemical box model, the locally-produced and regionally-transported O_3, as well as their variation trends, were determined (see section 2.5).

The PBM-MCM simulates the in-situ O_3 photochemistry based on the observed O_3 precursors. Figure S2 shows the average mixing ratios of some O_3 precursors in different wind sectors. The higher levels of CO, ethyne, ethane, propane and toluene under northwest winds indicated the transport of these species from PRD to Hong Kong. Meanwhile, O_3 might also be transported to Hong Kong. Text S1 discusses the determination of the locally produced and regionally transported O_3, as well as the uncertainties.

For details, please refer to lines 303-308, page 13.

Text S1. Determination of the locally produced and regionally transported O_3 and discussion on the uncertainties.

As an observation based model, PBM-MCM has been widely used to simulate the in-situ O_3 production (Lam et al., 2013; Ling et al., 2014; Lyu et al., 2017b; Wang et al., 2017a). Therefore, the O_3 simulated by PBM-MCM can be regarded as the locally produced O_3, and the differences between the observed and simulated O_3 were taken as the regionally transported O_3. However, it should be noted that the observed concentrations of O_3 precursors could be partially built up by regional transport. For example, under the northwest winds, the average mixing ratios of CO (693.9 ±25.5 ppbv), ethyne (2.15 ±0.22 ppbv), ethane (2.31 ±0.25 ppbv), propane (2.97 ±0.51 ppbv) and toluene (2.42 ±0.52 ppbv) were the highest among all the wind sectors, surpassing their average concentrations under light winds (wind speeds < 2 m/s) by 11.3%, 48.0%, 42.5%, 53.5% and 138.5%, respectively. Since the PBM-MCM was constrained by the observed concentrations of O_3 precursors, the share of regionally

transported O_3 precursors in the observations made contributions to the simulated O_3, which in fact represented a kind of regional transport. Therefore, the locally produced O_3 was to some extent overestimated in this way. Conversely, the regionally transported O_3 was underestimated. However, it is difficult to accurately quantify the contributions of regional transport to O_3 precursors at the site. Moreover, due to the non-linear relationships between O_3 and its precursors, we did not quantitatively evaluate the overestimation of the locally produced O_3 and the underestimation of the regionally transported O_3.

For details, please refer to Figure S2 and Text S1.

iv) HONO was not monitored in 2016 and the 2011 values were used. Some justification, based on measurements elsewhere, is provided. Figure 7 shows the OH formation and loss rates and demonstrates the importance of HONO in the early morning, especially in 2016. The potential error in this rate analysis should be emphasized.

We are grateful for this excellent comment.

It is true that HONO is an important source of OH, particularly in the early morning when the nightlong secondarily formed HONO and the primarily emitted HONO in the morning rush hours are subject to photolysis in the presence of sunlight. However, it is pity that HONO was not measured in the three sampling campaigns. To our best knowledge, the HONO concentrations at the sampling site were only reported by Xu et al. (2015), based on the measurements in the autumn of 2011. Therefore, we used an average diurnal cycle of HONO measured by Xu et al. (2015) to constrain the HONO concentrations in the model. To evaluate the uncertainties of adopting the HONO concentrations in 2011, we calculated the average

diurnal cycles of HONO in the 2007, 2013 and 2016 sampling campaigns (Figure S5), according to the diurnal patterns of HONO/NO_x ratios determined at the same site (Xu et al., 2015) and real measurements of NO_x concentrations. It was found that by adopting the values in 2011, the HONO concentrations were underestimated by 14.9% and 11.6% in 2007 and 2013, respectively, but were overestimated by 10.4% 2016. Further, this caused the maximum underestimation (overestimation) of the total OH production rate by 2.3±2.3% (21.6±5.2%) in 2007, 5.8±1.3% (3.4±1.0%) in 2013 and 5.7±1.3% (3.4±0.9%) in 2016. It should be noted that the maximum overestimation of the total OH production rate in 2007 (21.6±5.2%) occurred at 07:00 LT when the OH recycling was weak. During 08:00 – 19:00 LT, both the underestimation and overestimation of the simulated total OH production rates were less than 3%. Overall, by adopting the measured HONO in 2011 at TC, the simulations of OH formation and loss rates were not largely biased.

Besides, the HONO concentrations calculated from the HONO/NO_x ratios and NO_x concentrations also had certain uncertainties. Thus, we did not use the calculated HONO concentrations to constrain the model. In fact, the consistent input of HONO concentrations in the three sampling campaigns enabled us to look into the changes of O_3 and radical photochemistry induced by the other factors, such as VOCs, NO_x and meteorological conditions.

Discussions are added in the main text and the supplement.

As stated in section 2.4.2, the average diurnal cycle of HONO measured at TC in 2011 was adopted in the simulations. To assess the uncertainties, we also calculated the HONO concentrations according to the measured HONO/NO_x ratios and the NO_x concentrations at TC

in the three sampling campaigns (Figure S5). The uncertainties in HONO concentrations and in the contributions of HONO to OH formation and loss rates are discussed in Text S3.

For details, please refer to lines 530-535, pages 24-25 and Text S3.

v) This last point illustrates one of the deficiencies of the paper – the tendency to discuss the behavior of average values and reaction rates rather than delve into the diurnal variations, which show some interesting effects, some difficult to understand. For example, in Fig 7, the high NO + HO_2 rate shows that the chain length is quite long, especially in 2007 – the propagation rate considerably exceeds the initiation rates (mainly O_3 + alkene and $O^1D + H_2O$). The OH production from HONO is large balanced by HONO formation from OH + NO except in the early morning. On the other hand, the termination rate (OH + NO2) is quite large and significantly exceeds the initiation rates. Why is this? It needs some explanation. The effects are still there in the later years, although less pronounced.

Thank you for the insightful and professional comments.

First of all, we must admit a careless mistake we made in plotting Figure 7. The legends of the OH loss pathways were misplaced. Besides, the measured concentrations of formaldehyde were forgotten to input into the model, which are now used to constrain the model in the revised manuscript. The changes of the numbers in sections 3.2 and 3.3 are almost due to the re-simulations performed with the input of formaldehyde concentrations into the model. Please refer to the updated Figure 7 for the further review on the revised manuscript and the responses below.

The high reaction rates between HO_2 and NO at the sampling site were also reported in

previous studies. For example, Xue et al. (2016) indicated that the formation rate of OH through HO_2 reacting with NO (12.5 ppbv/h) was nearly 5 times the total OH formation rate through the initial reactions (HONO photolysis, O_3 photolysis, O_3 + VOCs, H_2O_2 photolysis and HNO_3 photolysis) on an O_3 episode day at the same site. The high reaction rates between HO_2 and NO were mainly attributable to the sufficient HO_2 and NO at this suburban site. To verify, the formation and loss rates of OH at an island (WSI) more than 40 km away from Hong Kong (Wang et al., 2018a) were simulated. The simulation was performed on one day with low NO_x, when the island was dominated by the sea breezes. It was found that the reaction between HO_2 and NO only accounted for 42.7±0.2% of the OH formation rate, in contrast to 69.8±1.1% at TC.

The balance between HONO photolysis rates and the formation rates of HONO through NO reacting with OH was not either the truth, which was misleading information resulting from the mistakes in the Figure legend as we admitted. According to the updated Figure 7, the net OH production rates through HONO photolysis (the differences between the photolysis rates and formation rates of HONO) were $0.68\pm0.21 \times 10^6$, $0.70\pm0.12 \times 10^6$ and $0.87\pm0.12 \times 10^6$ molecules cm^{-3} s^{-1} in the 2007, 2013 and 2016 sampling campaigns, respectively.

With regard to the unreasonably high reaction rates of the termination reaction (OH + NO_2), we apologize again, because this was also wrong information resulting from the misplaced Figure legend. As shown in the updated Figure 7, OH was primarily consumed by reacting with VOCs, and the termination reaction rates were at the same magnitude as the initial reaction rates. Specifically, the initial formation rates of OH were higher than the reaction rates of OH + NO_2 in the early morning (7:00 – 10:00 LT), which was reversed in the following

hours of the day due to the enhanced OH productions through the propagation reaction. As a comparison, the model simulation indicated that the initial reaction rates were always higher than the termination reaction rates throughout a low NO_x day on WSI, with the average rate of $3.3 \pm 0.02 \times 10^7$ and $0.2 \pm 0.002 \times 10^7$ molecules cm^{-3} s^{-1}, respectively. This was reasonable, because the reactions among peroxy radicals take over the role of OH + NO_2 in terminating the reactions in low NO_x environments.

Based on the corrections and deeper analyses above, the discussions are also revised to delve into the diurnal variations rather than the average values of the OH formation and loss rates. Revisions have been made in the revised manuscript as follows.

Figure 7 presents the average diurnal profiles of the simulated OH and the formation and loss pathways dominating the recycling of OH during the three sampling periods, which roughly followed the typical pattern of the intensities of photochemical reactions, *i.e.* higher at noon and lower at the beginning and end of the day. On average, the simulated OH concentration was comparable (p=0.4) between the 2007 sampling campaign ($1.6 \pm 0.3 \times 10^6$ molecules cm^{-3}) and the 2013 sampling campaign ($1.5 \pm 0.2 \times 10^6$ molecules cm^{-3}), but it decreased (p<0.05) to $1.0 \pm 0.2 \times 10^6$ molecules cm^{-3} in the 2016 sampling campaign.

As expected, the formation and loss rates of OH were basically balanced in all the cases. OH was mainly formed from the reaction of HO_2+NO, which accounted for 69.8 ±1.1% of the total OH production rate over the three sampling campaigns. The photolysis of HONO ranked the second in supplying OH with the contribution of 22.0 ±1.4%. As stated in section 2.4.2, the average diurnal cycle of HONO measured at TC in 2011 was adopted in the simulations. To assess the uncertainties, we also calculated the HONO concentrations according to the

measured HONO/NO_x ratios and the NO_x concentrations at TC in the three sampling campaigns (Figure S5). The uncertainties in HONO concentrations and in the contributions of HONO to OH formation and loss rates are discussed in Text S3. The formation of OH from HONO photolysis was most efficient in the early morning, which was explained by the morning peak of HONO concentration, due to the nocturnal heterogeneous formation and the vehicle emissions in morning rush hours. Apart from the two dominant pathways, O_3 photolysis (6.3±0.2%), ozonolysis of unsaturated VOCs (1.5±0.2%) and H_2O_2 photolysis (0.2±0.01%) also made some contributions to the formation of OH, with the highest rates at noon or in the early afternoon when the productions of O_3 and H_2O_2 were the most intensive. To sum up, the total formation rates of OH from the primary sources (photolysis of HONO, O_3 and H_2O_2, and ozonolysis of VOCs) were lower than the recycling rates of OH (HO_2+NO) throughout the day at TC, consistent with the results in Xue et al. (2016) simulated at the same site. The dominant role of HO_2+NO in OH formation at TC (average contribution of 69.8±1.1%) might be related to the abundant NO at this site. The same pathway was simulated and accounted for only 42.7±0.2% of the total OH formation rate at an island more than 40 km away from Hong Kong with very low NO concentrations, *i.e.* maximum of 0.56 ppbv (Wang et al., 2018a).

OH was mainly depleted by the reactions with VOCs (32.3±1.2%), NO_2 (31.9±0.9%), CO (19.3±0.6%) and NO (16.5±1.1%). The reaction rates of OH+NO (formation rates of HONO) had the highest values in the morning, approximately in line with the diurnal pattern of the HONO photolysis rates, which however were not completely balanced due to the constraint of HONO to observations in the model. The average net photolysis rates of HONO (differences

between the HONO photolysis and formation rates) were $0.68 \pm 0.21 \times 10^6$, $0.70 \pm 0.12 \times 10^6$ and $0.87 \pm 0.12 \times 10^6$ molecules cm^{-3} s^{-1} in the 2007, 2013 and 2016 sampling campaigns, respectively. The losses of OH through the other pathways all exhibited the highest efficiencies at noon or in the early afternoon. It should be noted that the reaction between OH and NO_2 was not only the sink of OH but also a termination reaction in the photochemical system. In comparison, the termination reaction rates were lower than the OH formation rates from the primary sources (photolysis of HONO, O_3 and H_2O_2, and ozonolysis of VOCs) in the morning (7:00 – 10:00 LT), which were reversed in the following hours of the day due to the increases in OH concentrations.

For detail, please refer to lines 520-564, pages 24-26, Figure S5 and Text S3.

vi) It would help understand these arguments, and those given on page 25, if Fig S3 were shown, and discussed in more detail, in the main text. Why do the concentrations of HO_2 and RO_2 increase in the late afternoon in 2016?

Thank you for the suggestion.

We hope that most of the reviewer's concerns on these arguments have been addressed in the response to comment (v). The increases of HO_2 and RO_2 concentrations in the late afternoon were caused by the abnormally high concentrations of some VOCs or OVOCs on a few days. For example, on Nov. 17, 2007, the mixing ratios of toluene substantially increased from 0.38 ppbv at 15:00 LT to 10.4 ppbv at 16:00. The increases were also observed for the concentrations of xylenes, *n*/*i*-butanes, *n*/*i*-pentanes and some other VOCs. This led to the jumping-up of the simulated RO_2 concentration from 1.7×10^7 molecule cm^{-3} s^{-1} at 15:00 LT to

4.5×10^{7} molecule cm^{-3} s^{-1} at 16:00 LT. Similarly, the increases of VOC concentrations occurred on some days in 2016, such as ethylbenzene, xylenes and isoprene on Sept. 26, isoprene on Oct. 16 and propionaldehyde on Nov. 7.

Note that the NO concentrations at 16:00 LT were generally low, due to the photochemical consumption. As a result, HO_2 and RO_2 produced by the substantially elevated VOC concentrations could not be efficiently converted to OH and RO, causing the rebounding of these peroxy radicals. Since the sources of VOCs in the atmosphere were complicated and these high VOC concentrations could not be simply treated as outliers, we did nothing to the simulated HO_2 and RO_2 but explained the rebounding phenomenon in the caption of Figure S6. To avoid over complication of the main text, we did not move Figure S6 (original Figure S3) to the main text.

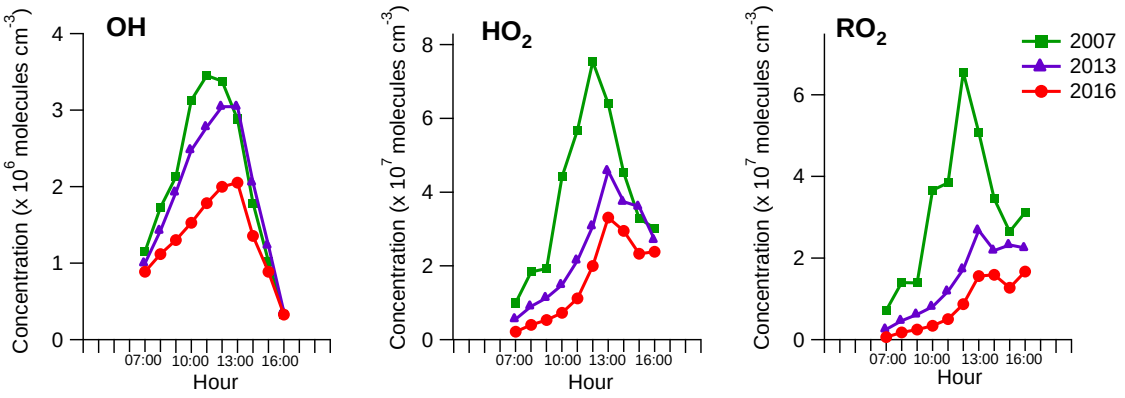

Figure S6. Average diurnal profiles of the simulated OH, HO_2 and RO_2 concentrations on VOC sampling days in 2007, 2013 and 2016. The rebounding of HO_2 and RO_2 concentrations in the late afternoon in 2007 and 2016 was caused by the substantial increases in the concentrations of some VOCs or OVOCs in several samples.

For details, please refer to Figure S6.

vii) The concentrations of oxygenates are very high (Table S4), yet their sources are not discussed in the main text. Are they produced by reaction or are there emission sources? Were the concentrations constrained, or were they simulated? Were high concentrations of other oxygenates generated in the simulations?

Thanks for the questions.

Yes, the concentrations of carbonyls (oxygenates) were on high levels. Though their sources were beyond the scope of this study, Guo et al. (2013b) and Ling et al. (2016b) indicated that secondary formation accounted for large fractions of the ambient formaldehyde (60-76%), acetaldehyde (45-53%) and acetone (~71%) in Hong Kong, leaving the rest to be contributed by 24-40%, 47-55% and ~29%, respectively. The concentrations of formaldehyde, acetaldehyde, acetone and propionaldehyde were constrained to observations in the model, while the other carbonyls were simulated by the model. The average simulated mixing ratios of methyl ethyl ketone (0.17 ±0.02 ppbv), methacrolein (0.12 ±0.01 ppbv), butyraldehyde (0.02 ±0.003 ppbv) and acrolein (0.02 ±0.004 ppbv) on all the VOC sampling days across the three sampling campaigns were in general lower than those reported in previous studies (Ho et al., 2002, 2007; Cheng et al., 2014), implying the sources of these OVOCs other than secondary formation. However, due to the low detection rates of these OVOCs in the samples, it is not reasonable to constrain their concentrations to the observations.

Clarifications have been made in the revised manuscript as follows.

Though previous studies (Guo et al., 2013b; Ling et al., 2016b) indicated that secondary formation dominated the sources of OVOCs in Hong Kong, the primary emissions could not be neglected. Therefore, formaldehyde, acetaldehyde, acetone and propionaldehyde with

relatively high abundances were constrained to the observed concentrations in the model, while the other OVOCs with low concentrations and low detection rates were simulated by the model.

For details, please refer to lines 268-273, pages 12.

viii) Why were the BVOC concentrations so low in 2007 (Fig S4)? The temperature was slightly lower, but not by much, and the solar irradiance was high (Table S5).

Thanks for the question.

The low concentrations of BVOC in 2007 shown in Figure S7 (original Figure S4) were consistent with the low levels of isoprene (Table S5). Figure S8 shows the relationship between the common logarithm of isoprene mixing ratios and temperature. It is found that the higher temperatures corresponded to higher mixing ratios of isoprene, and the data points in 2007 did not deviate from the data points in 2013 and 2016, suggesting that the lower isoprene mixing ratios in 2007 were mainly attributable to the lower temperature.

In addition, the average wind speed in 2007 (2.3 ± 0.2 m s^{-1}) was much higher ($p<0.05$) than those in 2013 (1.0 ± 0.1 m s^{-1}) and 2016 (0.9 ± 0.1 m s^{-1}), with more frequent southeast winds in 2007 (62.8%). The strong winds from South China Sea might dilute isoprene emitted from the terrestrial plants, partially responsible for the low isoprene levels in 2007.

Explanation to the lower BVOCs in 2007 is given in the revised manuscript.

At last, the increase of BVOCs from 2007 to 2013 but comparable levels between 2013 and 2016 seemed to be related to the lower ($p<0.05$) temperature in the 2007 sampling campaign (Figure S8 and Table S6). Besides, the more frequent (62.8%) southeast winds from SCS with

higher wind speeds (2.3±0.2 m s^{-1}) might dilute BVOCs emitted from the terrestrial plants in the 2007 sampling campaign.

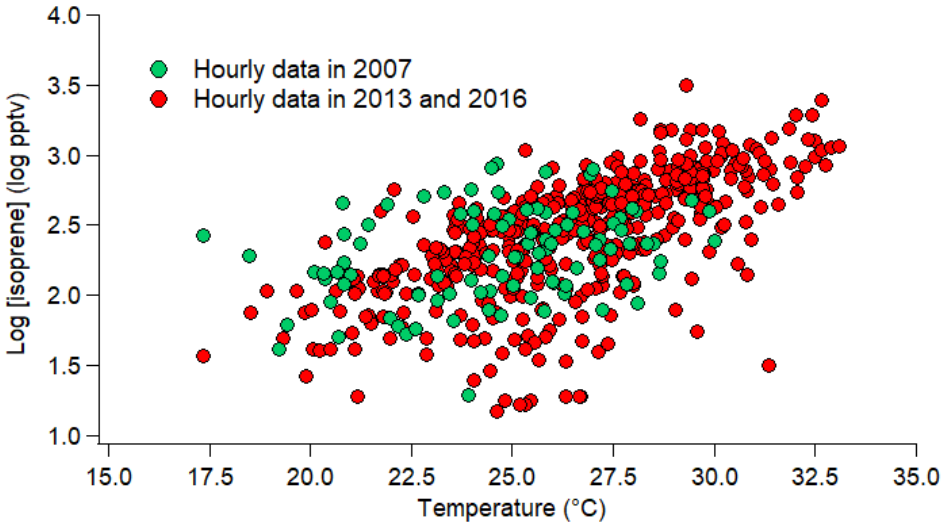

Figure S8. Relationship between the common logarithm of isoprene mixing ratios and temperature.

For details, please refer to lines 644-648, page 30 and Figure S8 and Table S6.

ix) While the analysis of the impact on O_3 of the emissions changes, via the scenario B simulations, is of considerable value, it is important, once again, to point out that the chemistry is non-linear, and the approach limits the quantitative, but not the qualitative, nature of the conclusions.

We thank for the good suggestion.

Indeed, due to the non-linearity of O_3 photochemistry, the contributions to the simulated O_3 of the individual sources determined by the subtraction approach were only the qualitative but not quantitative evaluations.

This has been clarified in the revised manuscript as follows.

It should be noted that due to the nonlinear relationships between O_3 and its precursors, the subtraction approach only qualitatively rather than quantitatively evaluated the contributions of VOC sources to O_3 production.

For details, please refer to lines 320-322, pages 14.

x) Small point: the decrease in [OH] of less than 10% between 2007 and 2013 could hardly be described as significant (p24, line 502).

Accepted with thanks. It has been checked that the decrease of OH concentrations from 2007 to 2013 was insignificant, where p=0.4. Revisions have been made in the manuscript.

On average, the simulated OH concentration was comparable (p=0.4) between the 2007 sampling campaign ($1.6 \pm 0.3 \times 10^6$ molecules cm^{-3}) and the 2013 sampling campaign ($1.5 \pm 0.2 \times 10^6$ molecules cm^{-3}), but it decreased (p<0.05) to $1.0 \pm 0.2 \times 10^6$ molecules cm^{-3} in the 2016 sampling campaign.

For details, please refer to line 524-527, page 24.

Some of these comments require relatively detailed responses, which may need to be consigned to the Supplement to avoid over complication of the main text. It is important, though, that the issues related to the detailed chemistry are resolved since much of the emphasis of the paper depends on the box model calculations.

Again, we express our sincere appreciation to the reviewer for his/her insightful and professional comments & suggestion. We realized the importance of addressing the problems related to the detailed chemistry in this paper and made efforts to improve the paper through

correcting the mistakes (such as the big mistake in the legend of Figure 7), mining the data and deepening the discussion. As suggested, additional supporting information is provided in the Supplement to avoid the over complication of the main text. Hope that the revised manuscript is satisfactory to be published.

References

Cheng, Y., Lee, S. C., Huang, Y., Ho, K. F., Ho, S. S. H., Yau, P. S., Louie, P. K. K., and Zhang, R. J.: Diurnal and seasonal trends of carbonyl compounds in roadside, urban, and suburban environment of Hong Kong, Atmos. Environ., 89, 43-51, 2014.

Guo, H., Ling, Z. H., Cheung, K., Jiang, F., Wang, D. W., Simpson, I. J., Barletta, B., Meinardi, S., Wang, T. J., Wang, X. M., Saunders, S. M., and Blake, D. R.: Characterization of photochemical pollution at different elevations in mountainous areas in Hong Kong, Atmos. Chem. Phys., 13, 3881-3898, 2013a.

Guo, H., Ling, Z. H., Cheung, K., Wang, D. W., Simpson, I. J., and Blake, D. R.: Acetone in the atmosphere of Hong Kong: Abundance, sources and photochemical precursors, Atmos. Environ., 65, 80-88, 2013b.

Ho, K. F., Lee, S. C., Louie, P. K., and Zou, S. C.: Seasonal variation of carbonyl compound concentrations in urban area of Hong Kong, Atmos. Environ., 36, 8, 1259-1265, 2002.

Ho, K. F., Ho, S. S. H., Cheng, Y., Lee, S. C., and Yu, J. Z.: Real-world emission factors of fifteen carbonyl compounds measured in a Hong Kong tunnel, Atmos. Environ.t, 41, 8, 1747-1758, 2007.

Lam, S. H. M., Saunders, S. M., Guo, H., Ling, Z. H., Jiang, F., Wang, X. M., and Wang, T. J.:

Modelling VOC source impacts on high ozone episode days observed at a mountain summit in Hong Kong under the influence of mountain-valley breezes, Atmos. Environ., 81, 166-176, 2013.

Li, K., Jacob, D. J., Liao, H., Shen, L., Zhang, Q., and Bates, K. H.: Anthropogenic drivers of 2013–2017 trends in summer surface ozone in China, Proc. Natl. Acad. Sci. U. S. A., 116, 2, 422-427, 2019.

Ling, Z. H. and Guo, H.: Contribution of VOC sources to photochemical ozone formation and its control policy implication in Hong Kong, Environ. Sci. Policy, 38, 180-191, 2014.

Ling, Z., Guo, H., Chen, G., Lam, S. H. M., and Fan, S.: Formaldehyde and acetaldehyde at different elevations in mountainous areas in Hong Kong, Aerosol Air Qual. Res., 16, 1868-1878, 2016b.

Lyu, X. P., Guo, H., Wang, N., Simpson, I. J., Cheng, H. R., Zeng, L. W., Saunders, S. M., Lam, S. H. M., Meinardi, S., and Blake, D. R.: Modeling C_1-C_4 alkyl nitrate photochemistry and their impacts on O_3 production in urban and suburban environments of Hong Kong, J. Geophys. Res. Atmos., 122, 10539-10556, 2017b.

Wang, H., Lyu, X. P., Guo, H., Wang, Y., Zou, S. C., Ling, Z. H., Wang, X. M., Jiang, F., Zeren, Y. Z., Pan, W. Z., Huang X. B., and Shen, J.: Ozone pollution around a coastal region of South China Sea: Interaction between marine and continental air, Atmos. Chem. Phys., 18, 4277-4295, 2018b.

Wang, Y., Wang, H., Guo, H., Lyu, X. P., Cheng, H. R., Ling, Z. L., Louie, P. K. K., Simpson, I J., Meinardi, S., and Blake, D. R.: Long-term O_3- precursor relationships in Hong Kong: field observation and model simulation, Atmos. Chem. Phys., 17, 10919-10935, 2017a.

Wang, Y., Guo, H., Zou, S. C., Lyu, X. P., Ling, Z. H., Cheng, H. R., and Zeren, Y. Z.: Surface O_3 photochemistry over the South China Sea: Application of a near-explicit chemical mechanism box model, Environ. Pollut., 234, 155-166, 2018a.

Xu, Z., Wang, T., Wu, J., Xue, L., Chan, J., Zha, Q., Zhou, S., Louie, P. K., and Luk, C. W.: Nitrous acid (HONO) in a polluted subtropical atmosphere: Seasonal variability, direct vehicle emissions and heterogeneous production at ground surface, Atmos. Environ., 106, 100-109, 2015.

Xue, L. K., Wang, T., Louie, P. K., Luk, C. W., Blake, D. R., and Xu, Z.: Increasing external effects negate local efforts to control ozone air pollution: a case study of Hong Kong and implications for other Chinese cities, Environ. Sci. Technol., 48, 10769-10775, 2014a.

Xue, L. K., Gu, R. R., Wang, T., Wang, X. F., Saunders, S., Blake, D., Louie, P. K. K., Luk, C. W. Y., Simpson, I., Xu, Z., Wang, Z., Gao, Y., Lee, S. C., Mellouki, A., and Wang, W. X.: Oxidative capacity and radical chemistry in the polluted atmosphere of Hong Kong and Pearl River Delta regional analysis of a severe photochemical smog episode, Atmos. Chem., Phys., 16, 9891-9903, 2016.

Inter-comparison of O_3 formation and radical chemistry in the past decade at a suburban site in Hong Kong

Xufei Liu[1,#], Xiaopu Lyu[1,#], Yu Wang[1], Fei Jiang[2], Hai Guo[1,*]

[1] Air Quality Studies, Department of Civil and Environmental Engineering, The Hong Kong Polytechnic University, Hong Kong, China

[2] Jiangsu Provincial Key Laboratory of Geographic Information Science and Technology, International Institute for Earth System Science, Nanjing University, Nanjing, China

*Corresponding author. ceguohai@polyu.edu.hk

# Both authors made equal contribution.

Abstract

Hong Kong, as one of the densely populated metropolises in East Asia, has been suffering from severe photochemical smog in the past decades, though the observed nitrogen oxides (NO_x) and total volatile organic compounds (TVOCs) were significantly reduced. This study, based on the observation data in the autumns of 2007, 2013 and 2016, investigated the photochemical ozone (O_3) formation and radical chemistry during the three sampling periods in Hong Kong with the aid of a Photochemical Box Model incorporating the Master Chemical Mechanism (PBM-MCM). While the simulated locally produced O_3 remained unchanged (p=0.73) from 2007 to 2013, the observed O_3 increased (p<0.05) at a rate of 1.78 ppbv/yr driven by the rise in regionally transported O_3 (1.77 ± 0.04 ppbv/yr). Both the observed and locally produced O_3 decreased (p<0.05) from the VOC sampling days in 2013 to those in 2016 at a rate of -5.31±0.07 and -5.52±0.05 ppbv yr^{-1}, respectively. However, a levelling-off (p=0.32) was simulated for the regionally transported O_3 during 2013 – 2016. The mitigation of autumn O_3 pollution in this region was further confirmed by the continuous monitoring data, which has never been reported in previous studies. Benefited from the air pollution control measures taken in Hong Kong, the local O_3 production rate decreased

remarkably (p<0.05) from 2007 to 2016, along with the lowering of recycling rate of hydroxyl radical (OH). Specifically, VOCs emitted from the source of liquefied petroleum gas (LPG) usage and gasoline evaporation decreased in this decade at a rate of -2.61±0.03 ppbv yr^{-1}, leading to a reduction of the O_3 production rate from 0.51±0.11 ppbv h^{-1} in 2007 to 0.10±0.02 ppbv h^{-1} in 2016. In addition, solvent usage made decreasing contributions to both VOCs (rate = -2.29±0.03 ppbv yr^{-1}) and local O_3 production rate (1.22±0.17 and 0.14±0.05 ppbv h^{-1} in 2007 and 2016, respectively) in the same period. All the rates reported here were for the VOC sampling days in the three sampling campaigns. It is noteworthy that meteorological changes also play important roles in the inter-annual variations of the observed O_3 and the simulated O_3 production rates. Evaluations with more data in longer periods are therefore recommended. The analyses on the decadal changes of the local and regional photochemistry in Hong Kong in this study may be a reference for combating China's national-wide O_3 pollution in near future.

Keywords: Ozone formation; Volatile organic compounds; Radical chemistry; Source apportionment; Control measures

1 Introduction

Ground-level ozone (O_3) is one of the most representative air pollutants in photochemical smog, produced through photochemical reactions between volatile organic compounds (VOCs) and nitrogen oxides (NO_x) in presence of sunlight (NRC, 1992; Jacob et al., 1999; Guo et al., 2017). It is well documented that O_3 is harmful to human health (Bell et al., 2004), crops (Wang et al., 2005) and natural ecosystems (Ashmore, 2005). Through the last 30 years, extensive efforts have been made by the local and federal governments to alleviate the tropospheric O_3 pollution around the world (NRC, 1992; NARSTO, 2000; Wang et al., 2017a; Wang et al., 2018a). Effectiveness has gradually shown in some countries/regions, such as

Switzerland, Germany, Ireland and eastern North America (Lefohn et al., 2010; Cui et al., 2011; Derwent et al., 2013; Parrish et al., 2014; Lin et al., 2017). In contrast, the O_3 levels in many places are still increasing or not decreasing at the expected rates, particularly in East Asia (Ding et al., 2008; Xu et al., 2008; Parrish et al., 2014; Xue et al., 2014a; Wang et al., 2017a).

Hong Kong, as one of the densely populated metropolises in East Asia, has been suffering from severe photochemical smog in the past decades, though the locally-emitted NO_x and total VOCs (TVOCs) were significantly reduced (Xue et al., 2014a; Ou et al., 2015; Lyu et al., 2016a; Wang et al., 2017a). On one hand, this indicates the non-linear relationship between O_3 and its precursors. On the other hand, in addition to local O_3 formation, the observed O_3 in Hong Kong is also influenced by the regional transport due to the proximity of the highly industrialized Pearl River Delta (PRD) region. Earlier studies revealed that the local O_3 production is typically limited by VOCs in urban and some suburban areas in Hong Kong (Zhang et al., 2007; Ling et al., 2014; Wang et al., 2017b). Namely, cutting VOCs emissions will reduce O_3 production, while the reduction of NO_x may cause an O_3 increment (Cheng et al., 2010, 2013; Guo et al., 2011; Wang et al., 2017a). Previous studies also documented that photochemical O_3 formation is dependent upon the ratios between TVOCs and NO_x (Sillman, 1999; Guo et al., 2013a; Ling et al., 2013), reactivity of VOC species (Zhang et al., 2007; Liu et al., 2008; Cheng et al., 2010) and the composition of NO_x (*i.e.* relative abundances of NO_2 and NO) (Richter et al., 2005; Xu et al., 2008; Wang et al., 2018a). Moreover, located in the subtropical region, Hong Kong has relatively high temperature and strong solar radiation, which are favourable for local O_3 formation. For regional transport, studies (Wang et al., 2001; Ding et al., 2004; Wang et al., 2017b) indicated that O_3 was generally built up in Hong Kong under the northerly winds, whereas it was often driven down by the sea breeze from South China Sea (SCS) and by the southwest monsoon in warm seasons. The contribution of

regional transport to O_3 in Hong Kong even reached 70% under the dominance of tropical cyclone (Huang et al., 2005), a typical synoptic condition conducive to severe O_3 pollution in the Northern Hemisphere (So and Wang, 2003; Huang et al., 2005; Lam et al., 2005). To improve the air quality in Hong Kong, a series of control measures aiming at restriction of VOC emissions have been implemented by Hong Kong government since 2007, which effectively reduced the concentrations of some VOCs, such as propane and *i*-/*n*-butanes emitted from taxis and public light buses fuelled by liquefied petroleum gas (LPG) (Lyu et al., 2016b), the aromatics mainly attributable to solvent usage, and the alkenes in association with diesel exhaust (Lyu et al., 2017a). As a result, Xue et al. (2014a) and Wang et al. (2017a) found that the locally produced O_3 decreased. However, the regional and super-regional transport of O_3 and its precursors from PRD and eastern China to Hong Kong had offset the decrease of the local O_3 production, resulting in an overall increase of the observed O_3 in Hong Kong from 2005 to 2013. Overall, the previous studies have greatly enhanced our understanding on O_3 pollution in Hong Kong, and details about the studies can be referred to in Table S1.

Despite many previous studies (Xue et al., 2014a, 2016; Ou et al., 2015; Lyu et al., 2016a; Wang et al., 2017a; Wang et al., 2018a), the inter-annual variations of the O_3 formation regimes and radical chemistry have yet been fully understood in Hong Kong. Additionally, the online measurement data used in previous long-term O_3 study might hamper the exact understanding of the local O_3 formation mechanisms, due to the unavailability of many reactive VOCs, such as formaldehyde. Besides, the trends of the local production and regional transport of O_3 were only updated to 2013 in previous studies (Xue et al., 2014a; Wang et al., 2017a). In fact, many measures were taken to reduce air pollutants' emissions in the latest years in Hong Kong and PRD. For examples, nearly 75% of the old catalytic converters on LPG-fuelled vehicles were renewed during September 2013 - May 2014. A

program to eliminate the pre-Euro IV diesel vehicles or to upgrade their emission standards to Euro IV was initiated in March 2014 and is still ongoing till 2019 at its third phase. In PRD, the second stage of the clean air controlling program was implemented in 2013 - 2015 (DGEPD, 2013). In 2014, the Guangdong provincial government has launched an Action Plan for Air Pollution Prevention and Control (MEE PRC, 2014), putting the emphases on the emission control of traffics, coal-fired power plants and industrial sources. Investigations on the post-2013 variations of the local O_3 production in Hong Kong and the regional impacts provide a good opportunity for us to examine the effectiveness of these local and regional measures.

The objectives of this study were to re-examine the O_3 trend in the pre-2013 and trace the O_3 evolution in the post-2013 in Hong Kong, and to explore the underlying mechanisms for the variations of O_3 formation and radical chemistry. With the aid of a photochemical box model, the locally produced and regionally transported O_3, as well as their variation trends, were determined (see section 2.5). Under the assumption that the local O_3 production in these years was changed due to a series of control measures in Hong Kong, we also aimed to evaluate the actual effectiveness of these control measures. China is suffering from severe O_3 pollution, almost second to none over the world. While O_3 began to decrease in most areas of North America and Europe, China's O_3 pollution was even aggravated in recent years. A series of air pollution control strategies have been implemented in China, though most of them were not specifically designed for O_3 abatement. Investigations on O_3 trends and the potential causes in Hong Kong would provide a good example of assessing the evolution of O_3 pollution and the effects of artificial interventions in China. In addition, the changes in the regional contribution to O_3 in Hong Kong determined in this study would throw light upon the variations of O_3 in China, particularly in South China. It is expected that this study would have some inspiration to the O_3 pollution control in other cities and regions in China.

2 Methodolgy

2.1 Sampling site

Hong Kong is located on the southern coast of China with Guangdong province to the north and Pearl River Estuary (PRE) to the northwest. The sampling site (22.29N, 113.94E), Tung Chung (TC), was in a newly-developed suburban area in western Hong Kong, with a population of ~77,400 in 2016 (CSD, 2011, 2018). The urban centre of Hong Kong is ~20 km northeast of TC. Hong Kong is dominated by the subtropical oceanic monsoon climate. During warm seasons, the prevailing winds mainly come from SCS at a relatively low speed (southwest winds). In cold seasons, the east and northeast winds are predominant. Generally, the sampling site receives relatively polluted air masses from mainland China, *i.e.* PRD region, Yangtze River Delta region and even North China between October and March, when high O_3 levels are often observed (Wang et al., 2009). Therefore, the samplings were mainly conducted in October and November in this study, except for 4 out of 45 sampling days in September. The sampling site was close to a highway linking to the Hong Kong International Airport (HKIA), and the HKIA was around 3 km to the north of the site. In addition, the local emissions from residential activities may modulate the air quality at this site. It was expected that O_3 at TC would be significantly influenced by NO emitted from the aforementioned sources. As shown in Figure S1, the O_3 titrated by NO (ΔO_3-1) was equivalent to 29.9±8.8%, 26.7±12.7% and 32.5±16.6% of the photochemically formed O_3 (ΔO_3-2) in the 2007, 2013 and 2016 sampling campaigns, respectively, confirming the importance of NO titration in modulating O_3 at the site. Figure 1 shows the locations of the sampling site (TC) and the 12 air quality monitoring stations in PRD, which witnessed the evolution of air quality in PRD over the last decade and is used to demonstrate the variations of regional O_3 in this study. More detailed description of the site can be found in our previous studies (Jiang et al., 2010: Cheng et al., 2010; Ling et al., 2013; Ou et al., 2015).

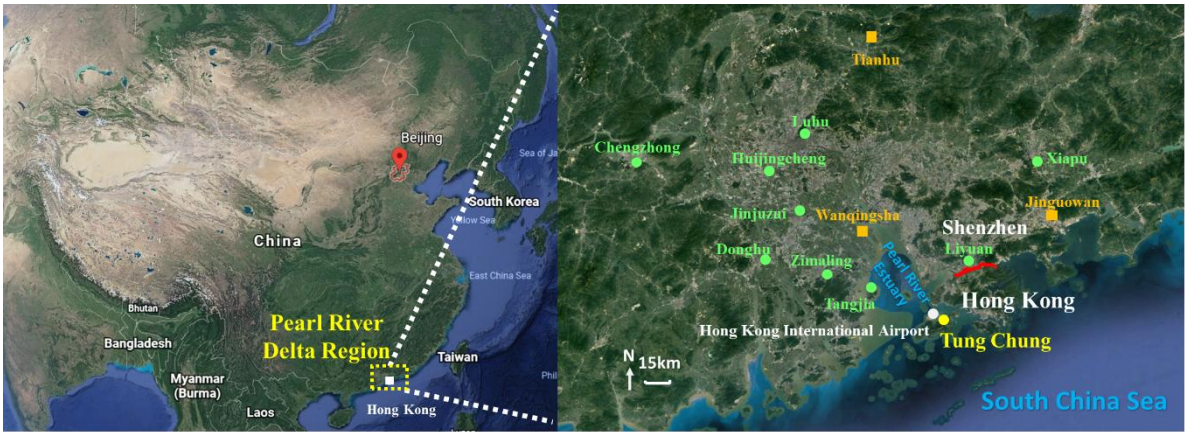

Figure 1. Location of the sampling site (yellow circle) and the surrounding environment. The red line in the right panel shows the border between Hong Kong and Shenzhen, Guangdong. The three regional and nine urban air quality monitoring stations in PRD are symbolized by orange blocks and green circles, respectively.

2.2 Continuous measurements of trace gases and collection of VOC/OVOC samples

Trace gases (SO_2, CO, NO, NO_2 and O_3) and meteorological conditions were continuously measured at TC site for three autumn periods in 2007, 2013 and 2016 (see Table S2 for the specific sampling periods), including 25 O_3 episode days with the maximum hourly average O_3 exceeding 100 ppbv (Level II of China National Ambient Air Quality Standard) and 185 non-episode days. VOC and OVOC samples were selectively collected on 8, 19 and 18 days in 2007, 2013 and 2016, respectively (see Table S2 for the specific sampling dates). The three sampling periods were used as representatives of the autumns in the three years in this study, and the rationality will be discussed in section 3.1.

Trace gases were continuously measured at the TC air quality monitoring station operated by the Hong Kong Environmental Protection Department (HKEPD), ~0.8 km to our sampling site. The instruments were the same as those used in the US air quality monitoring program (HKEPD, 2017a). Table S3 summarizes the instruments, analysis techniques, detection limits and the time resolutions for measurements of the trace gases. The high resolution data were

169 collected and averaged into the hourly averages. All the analysers except O_3 analyser were
170 zeroed daily by analysing scrubbed ambient air and calibrated every two weeks by a span gas
171 mixture with a NIST (National Institue of Standards and Technology) traceable standard,
172 while the O_3 analyser was calibrated using a transfer standard (Thermo Environmental
173 Instruments (TEI) 49PS) every two weeks. Details about the quality assurance and control
174 procedures can be found in Ling et al. (2016a). The meteorological parameters, including
175 temperature, relative humidity, pressure, wind speed, wind direction, precipitation and solar
176 radiation, were also continuously monitored by a mini weather station (Vantage Pro TM &
177 Vantage Pro 2 Plus TM Weather Stations, Davis Instruments) during the sampling periods.
178 Data were integrated into 30-minute averages by a built-in program in the weather station.
179 The collection and analysis of VOCs and OVOCs were detailed in our previous studies (Guo
180 et al., 2009; Wang et al., 2018b). Briefly, pre-cleaned and evacuated 2 L electropolished
181 stainless-steel canisters were used to collect VOC samples. On O_3 episode days, one-hour
182 sample was collected in each hour during the daytime (07:00-19:00 LT), generating 13
183 samples per day, while 5-7 one-hour samples were collected every other hour on non-O_3
184 episode days from 07:00 to 19:00 LT in the 2013 and 2016 sampling campaigns. However,
185 12 one-hour samples were collected on each VOC sampling day between 07:00 and 18:00 in
186 2007, regardless of O_3 episodes or non-episodes. The O_3 episode days were predicted prior to
187 sampling based on weather forecast and numerical simulation of O_3. Overall, the O_3 episodes
188 were usually associated with high temperature, strong solar radiation, low humidity, and
189 weak or northerly winds. A total of 414 canister samples, including 96 samples in 2007, 146
190 samples in 2013 and 172 samples in 2016, were collected and analysed during the three
191 sampling periods (Table S2).
192 In addition to VOC samples, OVOC samples were also collected on the same days as those
193 for the collection of VOCs. Dinitrophenylhydrazine (DNPH)-silica cartridges (Waters Sep-

Pak DNPH-Silica, Milford, MA) were used to collect the OVOC samples. An ozone scrubber (Sep-Pak; Waters Corporation, Milford, MA) was connected in front of the DNPH cartridge to prevent interference of ozone. The ozone scrubber was replaced every two OVOC samples. For each OVOC sample, air was drawn to pass the O_3 scrubber and the cartridge for 2 hours (2.5 hours in 2007 sampling campaign) at a flow rate of 0.5 L min^{-1}, which was controlled by a rotameter. During the sampling periods in 2013 and 2016, 5-7 OVOC samples were collected every two hours from 06:00-20:00 LT on both O_3 episode and non-episode days. In 2007, only 2 samples were collected on non-O_3 episode days at 10:30-13:00 and 13:00-15:30, and 4 samples between 08:00 and 18:00 on O_3 episode days. In total, 275 OVOC samples (28 in 2007, 124 in 2013 and 124 in 2016) were collected and analysed in the three sampling campaigns (Table S2).

2.3 Chemical analysis

2.3.1 Analysis of VOCs

The concentrations of 48 speciated non-methane hydrocarbons (NMHCs) in the canisters were determined with an Entech Model 7100 Preconcentrator (Entech Instruments Inc., California, USA) coupling with a gas chromatography-mass selective detector (Model 5973N, Agilent Technologies, USA), a flame ionization detector, and an electron capture detector (GC-MSD/FID/ECD). The NMHCs were analysed in Guangzhou Institute of Geochemistry (GIG), Chinese Academy of Sciences for the samples collected in both 2007 and 2013, and in The Hong Kong Polytechnic University (HKPolyU) for the samples collected in 2016. It should be noted that the GC-MSD/FID/ECD system in the latter two institutes was the same as that at UCI, and inter-comparisons were performed regularly among the three institutes, which showed reasonably good agreements (Ling et al., 2014; Wang et al., 2018b; Zeng et al., 2018). Detailed information about the analysis procedures and quality assurance and control

can be found in Colman et al. (2001) and Simpson et al. (2010). Table S4 summarizes the limits of detection (LoDs), precisions and accuracies of the VOC analyses in the three institutes.

The OVOC samples were stored in a refrigerator at 4 ℃ after sampling. For analyses of OVOCs, the cartridges were eluted slowly with 2 ml of acetonitrile into a 2-ml volumetric flask. A high-performance liquid chromatography (HPLC) system (Perkin Elmer Series 2000, MA, USA) coupled with an ultraviolet (UV) detector operating at 360 nm was used for analysis. The instrument was calibrated using standards of 5 gradient concentrations covering the concentrations of interest for different OVOCs in ambient air. Good linear relationships (R^2> 0.999) between the standard concentrations and responses of the instrument were obtained for the 16 analysed OVOC species. The built-in computerized programs of quality control systems such as auto-linearization and auto-calibration were used to guarantee the data quality. Detailed information about the analysis and quality control of OVOC samples was provided in Cheng et al. (2014), Cui et al. (2016) and Ling et al. (2016b). Due to the low detection rate of many OVOCs, this study only focused on formaldehyde, acetaldehyde, acetone and propionaldehyde, which had relatively high concentrations.

2.4 Model description

2.4.1 Positive matrix factorization (PMF)

PMF is a receptor model that has been extensively used for source apportionment of airborne particulate matters and VOCs (Lee et al., 1999; Brown et al., 2007). In this study, US EPA PMF 5.0 model (US EPA, 2017) was applied to identify the sources of O_3 precursors, according to Equation (1) (Paatero, 1997; Ling et al., 2014).

$$x_{ij} = \sum_{k=1}^{p} g_{ik} f_{kj} + e_{ij} \qquad \text{Equation (1)}$$

where x_{ij} is the measured concentration of *j*th species in *i*th sample, g_{ik} represents the contribution of *k*th source to *i*th sample, f_{kj} denotes the fraction of *j*th species in *k*th source, and e_{ij} is the residual for *j*th species in *i*th sample. *p* stands for the total number of independent sources (Paatero, 2000a, b).

The uncertainties of the concentrations applied to PMF were set in the same way as Polissar et al. (1998) and Reff et al. (2007). Values below or equal to the LoD were replaced by half of the LoDs and the uncertainties for these values were set as 5/6 of the corresponding LoDs. For the values greater than LoDs, the uncertainties were calculated as $[(\text{Error Fraction} \times \text{concentration})^2 + (\text{LoD})^2]^{1/2}$ where 10% was assigned as the error fraction. Missing values (mainly due to maintenance or malfunction of the instruments) were replaced by the geometric mean of the measured values and their accompanying uncertainties were set as four times the geometric mean value. More details about the settings of the uncertainty were provided in Norris et al. (2008) and Zhang et al. (2012).

The model was run for 20 times with a random seed, and tests with different number of factors were conducted. The optimum solution was finally determined based on both a good fit to the observed data and the most reasonable and interpretable results according to the knowledge on the sources of O_3 precursors in Hong Kong (Ling et al., 2011, 2014; Ou et al., 2015).

2.4.2 Observation-based model (OBM)

A photochemical box model coupled with the Master Chemical Mechanism (PBM-MCM) was used to simulate the photochemical O_3 formation on the VOC sampling days. In this study, MCM v3.2, a near explicit chemical mechanism consisting of 5,900 species and 16,500 reactions which fully describes the homogeneous gas phase reactions in the atmosphere (Jenkin et al., 1997, 2003; Saunders et al., 2003), was used. The observation data

of temperature, relative humidity, O_3, SO_2, CO, NO, NO_2 and 52 C_2-C_{10} VOCs/OVOCs were input into the model. Specifically, the 52 VOCs/OVOCs included 19 alkanes, 16 alkenes, 13 aromatics and 4 OVOCs, as shown in Table S5, where the statistics of the mixing ratios of VOCs/OVOCs are also presented. Though previous studies (Guo et al., 2013b; Ling et al., 2016b) indicated that secondary formation dominated the sources of OVOCs in Hong Kong, the primary emissions could not be neglected. Therefore, formaldehyde, acetaldehyde, acetone and propionaldehyde with relatively high abundances were constrained to the observed concentrations in the model, while the other OVOCs with low concentrations and low detection rates were simulated by the model. Nitrous acid (HONO) was not monitored in this study. The average diurnal cycle of HONO mixing ratios measured at the same site in autumn in 2011 (Xu et al., 2015) was input into the model to roughly represent its role in O_3 formation and atmospheric radical chemistry. Due to the data limitation, the trends of HONO at TC in the three sampling campaigns were not traceable. However, the measurements at a background site in Hong Kong indicated comparable levels of HONO (p>0.1) between the autumn in 2012 and in 2018 (unpublished data). Therefore, adopting the HONO measured in 2011 as the inputs of the simulations in the three sampling campaigns was likely a plausible assumption, despite some uncertainties. The model was also tailored to the real situations in Hong Kong. Specifically, the height of the planetary boundary layer was allowed to vary from 300 m at night to 1400 m at noon. The photolysis rates were calculated according to the measured solar radiations by the Tropospheric Ultraviolet and Visible Radiation model (Madronich and Flocke, 1999; Wang et al., 2017a), with the detailed method described in Lyu et al. (2017b). In addition to the chemical processes, the exchange between the lower troposphere and free troposphere, and dry deposition were also considered in the model. The concentrations of air pollutants in the free troposphere were set according to the observations at a mountainous site in Hong Kong (Lam et al., 2013). The dry deposition rates were

adopted from the previous studies (Saunders et al., 2003; Lam et al., 2013). The other physical processes were not included in the model, which might lead to insufficient description of the transport. However, since the model was constrained to the observations which included the transported air pollutants, the regional transport was partially considered. Besides, the observations at 07:00 on each day were used to initiate each day's modelling, through which the effect of regional transport before the daytime modelling was also considered. We admit that the PBM-MCM cannot perfectly reproduce the real atmospheric processes. However, it performed well in describing the in-situ photochemistry in previous studies (Lam et al., 2013; Ling et al., 2014; Lyu et al., 2017b; Wang et al., 2017a). Actually, the deficiency of PBM-MCM in consideration of the atmospheric dynamics enabled us to assess the contributions of regional transport to O_3 in Hong Kong, based on the differences between the observed and simulated O_3 (Wang et al., 2017a).

2.5 Simulation scenarios

The PBM-MCM simulates the in-situ O_3 photochemistry based on the observed O_3 precursors. Figure S2 shows the average mixing ratios of some O_3 precursors in different wind sectors. The higher levels of CO, ethyne, ethane, propane and toluene under northwest winds indicated the transport of these species from PRD to Hong Kong. Meanwhile, O_3 might also be transported to Hong Kong. Text S1 discusses the determination of the locally produced and regionally transported O_3, as well as the uncertainties. Furthermore, to evaluate the contributions of VOC sources to the local O_3 production, two scenarios of model simulation were performed, *i.e.*, Scenario A and Scenario B. The scenario A simulated the O_3 photochemistry in the whole air, which was constrained by the observed concentrations of all the O_3 precursors. The model simulations in scenario B (including six assumed sub-scenarios) were constrained by the concentrations of O_3 precursors with those contributed by individual sources being subtracted from the observed concentrations. Text S2 elaborates the set-up of

these scenarios. The simulated O_3 in scenario A was regarded as the locally produced O_3, as the observed O_3 concentrations were not input to constrain the model. Bearing in mind that the regional effects cannot be completely eliminated in this approach, due to the impacts of regional air on the observed concentrations of O_3 precursors. The differences between the scenario A and scenarios B reflected the contributions of the individual sources to the simulated O_3 production rate. It should be noted that due to the nonlinear relationships between O_3 and its precursors, the subtraction approach only qualitatively rather than quantitatively evaluated the contributions of VOC sources to O_3 production.

3 Results and discussion

3.1 Observation overview

Figure 2 shows the hourly mixing ratios of O_3 observed at TC in the autumns of 2007-2017 with the data on VOC sampling days being highlighted in red. It was found that the autumn O_3 increased significantly from 2007 to 2013 (p<0.01), with a rate of 0.34±0.002 ppbv yr^{-1}. This was consistent with Wang et al. (2017a) who reported an overall increase rate of autumn O_3 of 0.67±0.07 ppbv yr^{-1} at the same site for the period of 2005-2013. On one hand, the discrepancy in O_3 increasing rates might be due to the different statistics used to draw the rates, *i.e.* hourly values in this study and monthly averages in Wang et al. (2017a). On the other hand, the autumn O_3 increased substantially from 23.9±0.97 ppbv in 2005 to 30.2±0.97 ppbv in 2007, much quicker than the increase between 2007 and 2013. Without the inclusion of the period of 2005-2007 might be another reason of the less O_3 enhancement calculated here. In contrast to the increased autumn O_3 during 2007-2013, the autumn O_3 decreased obviously from 2013 to 2017 (p<0.01), at a rate of -2.27 ± 0.003 ppbv yr^{-1}, indicating a fundamental alleviation of O_3 pollution in Hong Kong in the latest 5 years. Overall, a statistically significant decreasing trend (rate = -0.44±0.001 ppbv yr^{-1}) was observed for the autumn O_3 at TC through 2007 to 2017 (p<0.05). The average O_3 on VOC sampling days in

the three sampling campaigns also followed the same pattern, which increased from 32.8±2.6 ppbv in 2007 to 36.9±2.3 ppbv in 2013, while decreased to 24.4±1.9 ppbv in 2016. Further, we investigated the number of O_3 episode days in the autumns of the three VOC sampling years (see Figure S3) and identified 15 (16.5% of the autumn days, same below) and 16 (17.6%) O_3 episode days in 2007 and 2013, respectively. However, there was only 5 (5.5%) O_3 episode days in the autumn of 2016. Similarly, the O_3 episode days accounted for 12.5%, 26.3% and 5.6% of the 2007, 2013 and 2016 sampling campaigns, respectively. Therefore, the increase of O_3 from 2007 to 2013 and the decrease in the following years could be represented by O_3 observed in the three sampling periods.

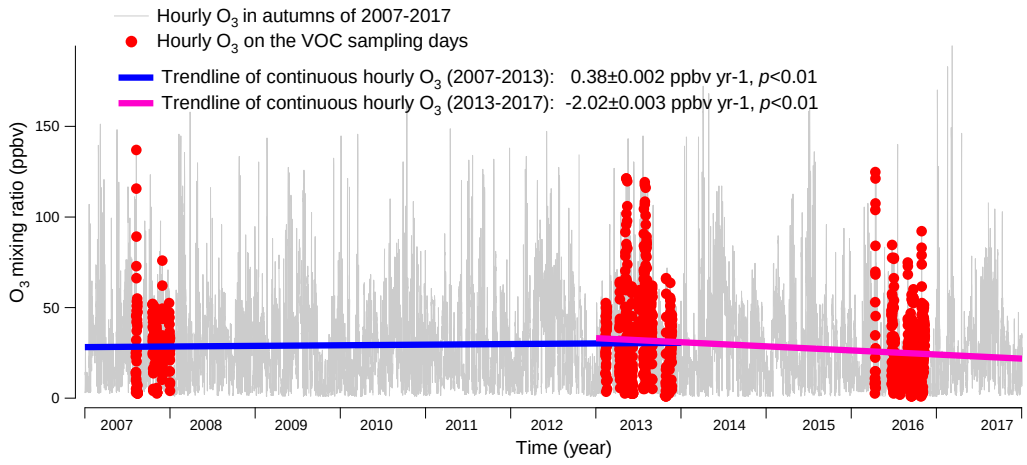

Figure 2. Long-term trends of the observed O_3 at TC from 2007 to 2017. Hourly O_3 values on the VOC sampling days in the autumns of 2007, 2013 and 2016 are marked in red. The hourly variation rates of O_3 are converted to yearly rates in periods of 2007 – 2013 and 2013 – 2017.

Table 1 and Table S6 present the observed O_3, CO, NO, NO_2, SO_2 and TVOCs, as well as the meteorological conditions averaged on the VOC sampling days in 2007, 2013 and 2016, respectively. From 2007 to 2013, the TVOCs decreased by nearly a half, which was expected to result in the reduction of O_3 in view of the VOC-limited regime of O_3 formation at TC (Cheng et al., 2010; Wang et al., 2017a). However, the increases of CO and the notable

decrease of NO in 2013 could enhance the O_3 production. The higher O_3 in 2013 indicated that this effect overrode the reduction of TVOCs in influencing the O_3 production. In particular, the decrease of NO meant the reduced NO titration to O_3, which has been recognized as a primary reason of O_3 increase in VOC-limited regime (Chou et al., 2006; Wang et al., 2018b). From 2013 to 2016, the decrease of O_3 was accompanied by the reductions of TVOCs and NO_2, though CO remained increasing at the same time. NO_2, as a direct source of O_3 through photolysis, plays important role in modulating the O_3 variation. Though the causes of NO_2 reduction are unknown to us, it might be one of the critical factors contributing to the decline of O_3 in Hong Kong in recent years. On the contrary, the increase of CO was also confirmed by the continuous monitoring data at TC, with a rate of 33.9 ± 0.7 ppbv yr^{-1} between 2013 and 2016. In fact, the consistent increasing trend ($p<0.05$) was also observed at the roadside sites in Hong Kong (not shown here). While the causes of CO increase in Hong Kong may be complicated, the increased vehicle emission is a plausible explanation. Studies (Johnson, 2008; Yao et al., 2008) revealed that while the new engine technologies performed well in reducing NO_x emission, they might lead to the increased emission of CO, with the application of lower air-to-fuel ratio and engine temperature.

In addition, studies have confirmed that continental anticyclones and tropical cyclones are conducive to severe O_3 pollution in Hong Kong, because these synoptic systems are often accompanied with northerly winds, high temperature, strong solar radiation, and relatively high pressure in Hong Kong (Ding et al., 2004; Huang et al., 2005; Jiang et al., 2015). Table S7 summarizes number of O_3 episode days with tropical cyclone, continental anticyclone and low pressure trough in the autumns of 2007, 2013 and 2016. In autumn 2007, 8, 8 and 1 O_3 episode day(s) were found to be related to the tropical cyclone, continental anticyclone and low-pressure trough, respectively, with 2 O_3 episode days under the combined influence of tropical cyclone and continental anticyclone. There were also 11 and 5

O_3 episode days in association with tropical cyclone and continental anticyclone in autumn 2013, respectively (Wang et al., 2018b). However, 4 out of the 5 episode days found in autumn 2016 were associated with tropical cyclone, with the other one related to low-pressure trough. Therefore, the lower O_3 and less O_3 episode days in 2016 were also benefited from the meteorological conditions.

Table 1. Mixing ratios of the measured trace gases and TVOCs averaged on the selective 45 VOC sampling days in 2007, 2013 and 2016.

	2007		**2013**		**2016**	
Unit: ppbv	Mean ± 95% C.I.	Max.	Mean ± 95% C.I.	Max.	Mean ± 95% C.I.	Max.
O_3	32.8 ±2.6	137.0	36.9 ±2.2	121.2	24.4 ±1.9	124.9
CO	456.3 ±19.8	847.0	585.0 ±11.9	1047.9	691.8 ±9.5	1074.7
NO	17.2 ±3.2	124.7	10.9 ±1.3	98.6	11.3 ±1.4	94.6
NO_2	27.7 ±2.1	69.6	31.5 ±1.4	80.8	22.0 ±1.1	103.2
SO_2	6.9 ±0.4	21.8	7.0 ±0.2	18.0	3.0 ±0.1	10.7
TVOCs	49.7 ±4.4	111.1	25.1 ±1.4	68.0	21.1 ±1.4	71.9

3.2 Model simulation of O_3

3.2.1 Model validation

Figure 3 compares the simulated O_3 in scenario A and the observed O_3 on the VOC sampling days. Overall, both the magnitudes and the temporal patterns of the observed O_3 were reasonably reproduced, though the mean of the simulated O_3 (33.8 ±1.9 ppbv) was slightly lower than the observed average (37.1 ±2.0 ppbv). To quantitatively evaluate the model performance, the index of agreement (IOA) was used to examine the goodness of fit between simulated and observed O_3. Within the range of 0-1, higher IOA represents better agreement

between the simulated and observed values (Willmott, 1982). In this study, the overall IOA for the three sampling periods was 0.74, within the range of IOA (0.67-0.89) accepted by the previous studies (Wang et al., 2015; Lyu et al., 2015, 2016a, c; Wang et al., 2017a, 2018a). Good correlations (R^2=0.61) were also shown between the simulated and observed hourly O_3. Bearing in mind the deficiencies of the box model in describing the atmospheric dynamics, we believed that the modelling results were acceptable, but special attention and explanation to the discrepancies between the simulated and observed O_3 was needed.

It was found that the discrepancies were most likely caused by the transport processes, *i.e.*, vertical and horizontal transport, which were not fully represented in the PBM-MCM model (George et al., 2013; Lakey et al., 2015; Wang et al., 2017a). For example, the simulated O_3 (maximum: 122.6 ppbv) was much higher than the observed O_3 (maximum: 44.3 ppbv) on November 16, 2007, when the strong southeast winds (wind direction: 90°-180°) with the highest wind speed of 5.3 m s^{-1} prevailed in Hong Kong. The south sector winds from SCS might dilute the locally produced O_3 and the O_3 precursors/intermediates (such as the radicals) which were not constrained by the observations. The same circumstances were also observed on October 27, November 17, 2007 and September 11-12, November 20, 2013, with southeast winds dominated (74.4%) during the daytime (Figure 3). For those days with the simulated O_3 lower than the observed O_3, *i.e.* October 3, 22-25, 2013 and November 6, 2016, 69.3% of the winds during the daytime came from the north (wind directions: 0-90° and 270°-360°), which might transport the air masses laden with O_3 and/or O_3 precursors/intermediates not constrained to the observations from inland PRD to the sampling site. The observed O_3 mixing ratios are plotted against the wind fields in Figure S4. It is obvious that O_3 were higher under the north winds, while lower in the south wind sectors, confirming the effects of dilution and regional transport of the south and north winds on O_3 pollution in Hong Kong, respectively.

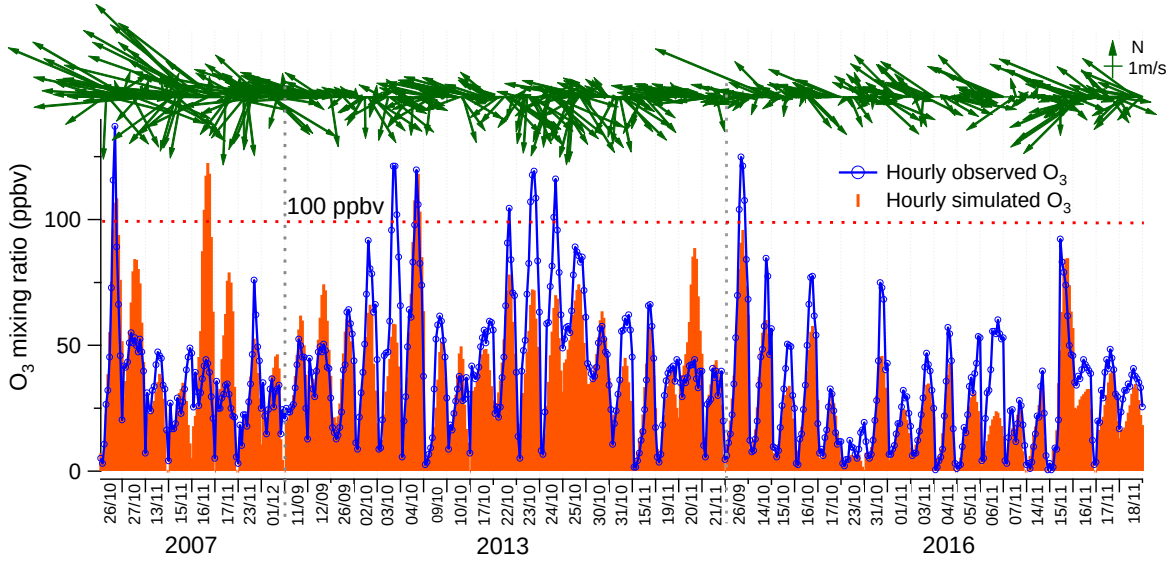

Figure 3. Hourly mixing ratio of the simulated and observed O_3 at TC during the VOC sampling periods in 2007, 2013 and 2016. The arrows represent the hourly wind sectors monitored at the sampling site.

3.2.2 Inter-annual variations of the locally produced and regional transported O_3

As discussed in section 2.5, the simulated O_3 in scenario A could be regarded as the locally produced O_3. Therefore, the differences between the observed O_3 and O_3 simulated in scenario A were treated as the regionally transported O_3 (Wang et al., 2017a). It is noteworthy that some negative values were generated with this method, corresponding to the dilution of the south winds to the locally produced O_3 as elaborated in section 3.2.1. Figure 4 shows the hourly mixing ratios of the observed, local and regional O_3 at TC in daytime hours (07:00-19:00 LT) of the three sampling campaigns. Overall, the observed O_3 was mainly (88.7±2.5%) contributed by the local photochemical production, with regional transport only accounting for 11.3±2.5% of the observed daily maximum O_3. However, regional transport was responsible for as high as 58.0±5.4% of the observed daily maximum O_3 in Hong Kong on the O_3 episode days when northerly winds prevailed, indicating the heavy O_3 burden superimposed by regional air masses from PRD. From 2007 to 2013, the simulated locally-produced O_3 remained statistically unchanged (p>0.1), in contrast to the increase of observed

O_3 and regional O_3 at rates of 1.78±0.05 ppbv yr^{-1} (p<0.05) and 1.77±0.04 ppbv yr^{-1} (p<0.05), respectively, the same trends as those reported by Wang et al. (2017a) for the autumn O_3 during 2005-2013. However, the decease of the locally produced O_3 in the same period as that simulated by Wang et al. (2017a) was not seen here according to the simulated O_3 in the 2007 and 2013 sampling campaigns. This discrepancy was likely caused by the limited samples in this study, no OVOCs considered in Wang et al. (2017a) and/or the inexactly same study periods between the two studies. Instead, we found that the locally produced O_3 showed a significant decline at a rate of -5.52±0.05 ppbv yr^{-1} during 2013-2016 (p<0.05), when the regionally transported O_3 did not change (p=0.32), resulting in a downward trend (-5.31±0.07) of the observed O_3. As such, the increase of the observed O_3 from 2007 to 2013 was reversed by the decrease between 2013 and 2016, leading to an overall decreasing trend of the observed O_3 during 2007-2016 (rate = -0.57±0.03 ppbv yr^{-1}, p<0.05).

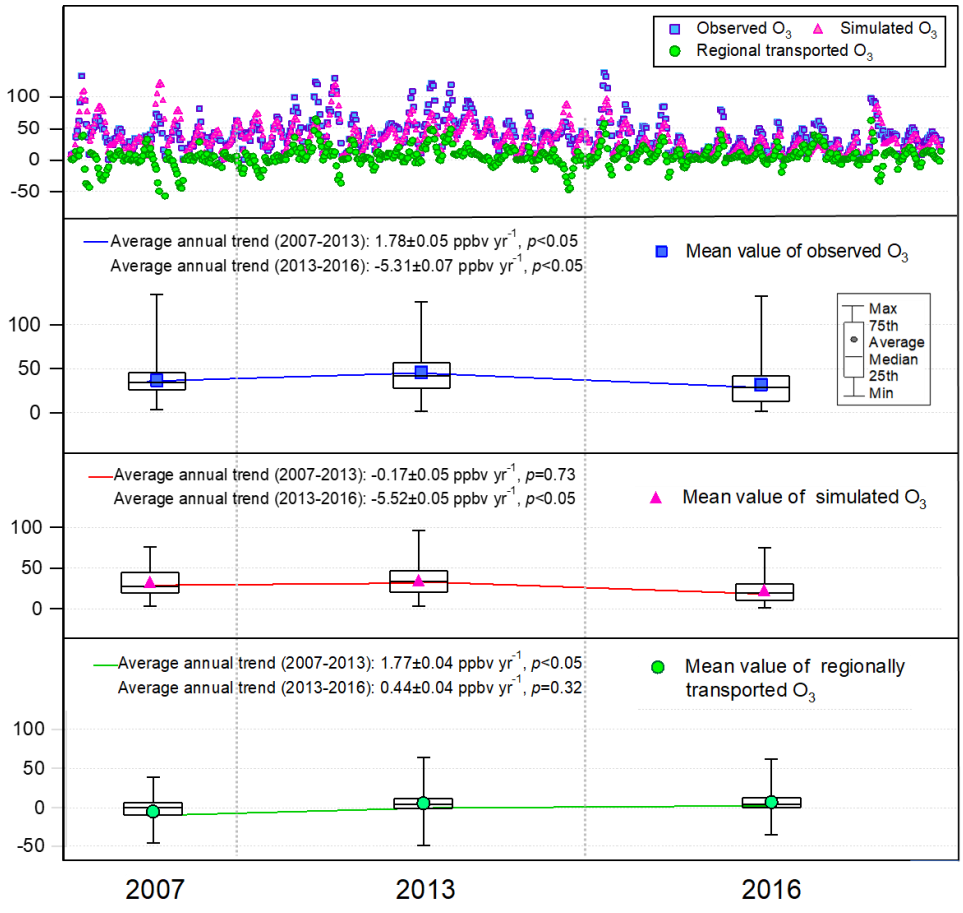

Figure 4. Hourly values (first panel) and the throughout-campaign statistical results (second to fourth panels) of the observed, simulated (locally-produced) and regional O_3 mixing ratios in daytime hours (07:00 – 19:00 LT) in the three sampling campaigns.

The significant alleviation of O_3 pollution in Hong Kong from 2013 to 2016 might be related to the measures taken to control the emissions of O_3 precursors in Hong Kong and in mainland China. The effectiveness of the actions launched by Hong Kong government in O_3 abatement was fully demonstrated in previous studies (Xue et al., 2014a; Lyu et al., 2017a; Wang et al., 2017a), and would be further evaluated in this study (section 3.4). Besides, the emission controls in mainland China might contribute to the decrease of O_3 or at least lessen the regional O_3 burden in this period. For example, the China's NO_x emissions for the first time showed a decreasing trend from 2013, benefited from the implementation of the China's Clean Air Action Plan (Zheng et al., 2018). Furthermore, we looked into the monthly average O_3 observed at the 12 air quality monitoring stations across the inland PRD, including three regional monitoring stations, *i.e.* Tianhu, Wanqingsha and Jinguowan, and nine urban monitoring stations, *i.e.* Xiapu, Jinjuzui, Donghu, Tangjia, Liyuan, Huijingcheng, Zimaling, Luhu and Chengzhong (https://www.epd.gov.hk/epd/sc_chi/resources_pub/publications/m_report.html). As shown in Figure 5, O_3 at these stations remained relatively stable (p=0.68) during 2006-2013, which however showed a contrastively decreasing trend at a rate of -1.27±0.25 ppbv yr^{-1} from 2013 to 2016. This corroborated our modelling results that the regional contribution to O_3 in Hong Kong ceased increasing or even began to decrease since 2013. While the substantial decrease of NO_x was a plausible reason for the alleviated regional O_3 pollution, meteorological variations might also play roles in modulating O_3 variations in these years (Li et al., 2019). However, analyses on the causes are out of the scope of this study. In addition to the reduced local formation and regional

transport of O_3, the more favourable meteorological conditions in 2016 might be another reason of the O_3 decrease, as discussed in section 3.1.

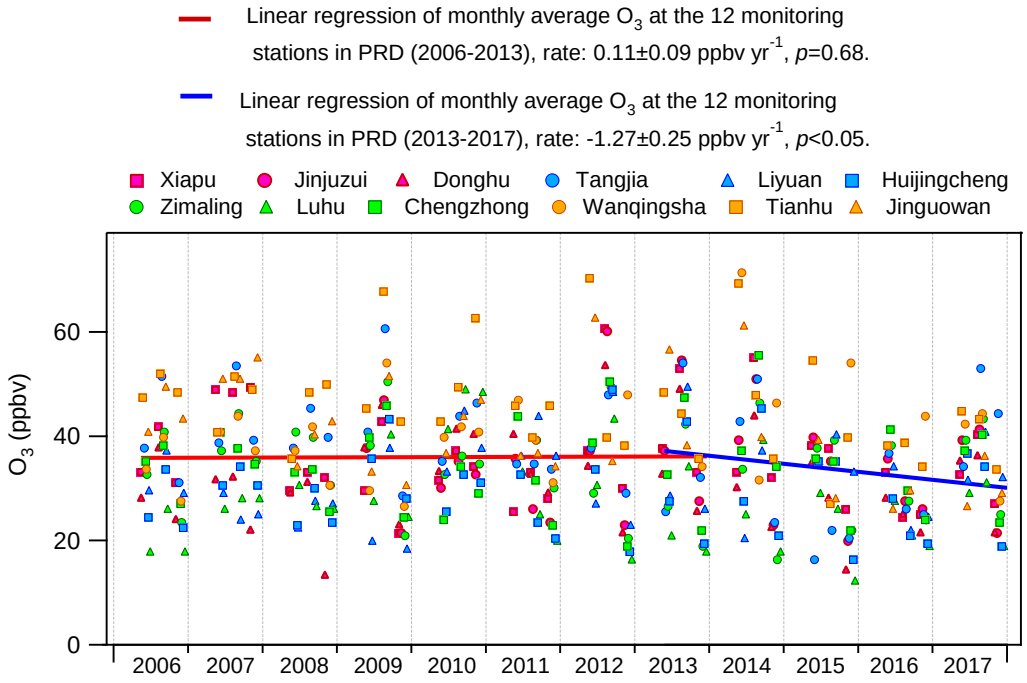

Figure 5. Trends of the observed monthly average O_3 at the 12 air quality monitoring stations in inland PRD.

3.3 Local production and destruction pathways of O_3 and OH radical

3.3.1 In-situ net O_3 production

Figure 6 shows the average diurnal profiles of the simulated O_3 production and destruction pathways during the three sampling campaigns. Also shown are the average diurnal cycles of the simulated O_3. The shift of the peaks between the net O_3 production rate and the simulated O_3 was due to the accumulation of the newly generated O_3 over time in the model, which was also true in the real situations. The reactions between NO_2 and O_3, leading to the formation of NO_3 and N_2O_5, in addition to dry deposition and aloft exchange, were the main depletions of the simulated O_3 in the late afternoon. Consistent with previous studies (Kanaya et al., 2009;

Liu et al., 2012; Xue et al., 2014b), these pathways were not included in the calculation of the net O_3 production rate, because we mainly focused on the photochemical processes in the hours when O_3 was accumulated. It was found that the reaction between HO_2 with NO dominated the O_3 production rates in all the cases, with an average rate of 3.7±0.7 ppbv h^{-1} (56.5±1.1%, percentage of the total O_3 production rate, same below), 2.5±0.3 ppbv h^{-1} (64.3±0.8%) and 1.4±0.2 ppbv h^{-1} (67.7±0.7%) in the 2007, 2013 and 2016 sampling campaigns, respectively. In addition, the sum of the reaction rates between RO_2 radicals and NO contributed 3.0±0.6 ppbv h^{-1} (43.5±1.1%), 1.5±0.2 ppbv h^{-1} (35.7±0.8%) and 0.7±0.1 ppbv h^{-1} (32.3±0.7%) to the O_3 production rate in 2007, 2013 and 2016, respectively. The formation of HNO_3 though the reaction between OH and NO_2 served as the main scavenger pathway of O_3, as NO_2 would be photolyzed and produce O_3 otherwise. On average, O_3 was consumed in this way at a rate of -1.3±0.2 ppbv h^{-1} (80.7±3.3%, percentage of the total O_3 destruction rate, same below), -1.0±0.1 ppbv h^{-1} (79.3±1.8%) and -0.6±0.07 ppbv h^{-1} (81.6±2.0%) in 2007, 2013 and 2016, respectively. The photolysis of O_3 was the second contributor to O_3 destruction, with an average contribution of -0.11±0.01 ppbv h^{-1} (8.5±0.5%) for the three sampling periods. Besides, the ozonolysis of unsaturated VOCs and the reactions between O_3 and radicals (OH and HO_2) were responsible for 3.5±0.3% and 1.7±0.2% of the total destruction rate of the locally produced O_3, respectively.

Overall, the net local O_3 production rate decreased from 5.2±1.1 ppbv h^{-1} in 2007, to 2.7±0.4 ppbv h^{-1} in 2013, till 1.4±0.3 ppbv h^{-1} in 2016, corresponding to the decline of the locally produced O_3 through 2007 to 2016 (Section 3.2.2).

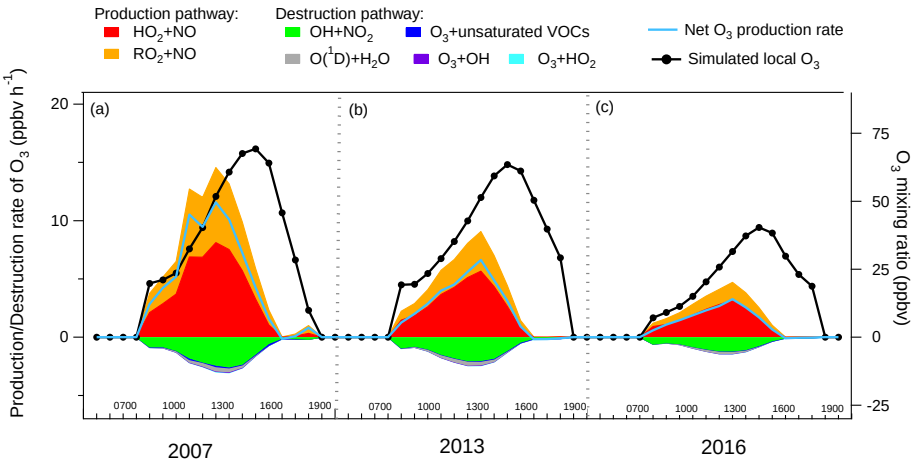

Figure 6. Average diurnal profiles of the local O_3 production and destruction rates in the sampling campaigns of (a) 2007, (b) 2013 and (c) 2016.

3.3.2 Recycling of OH radical

As one of the most important radicals in the atmosphere, OH initiates the oxidation of VOCs, leading to O_3 formation. Figure 7 presents the average diurnal profiles of the simulated OH and the formation and loss pathways dominating the recycling of OH during the three sampling periods, which roughly followed the typical pattern of the intensities of photochemical reactions, *i.e.* higher at noon and lower at the beginning and end of the day. On average, the simulated OH concentration was comparable (p=0.4) between the 2007 sampling campaign ($1.6 \pm 0.3 \times 10^6$ molecules cm^{-3}) and the 2013 sampling campaign ($1.5 \pm 0.2 \times 10^6$ molecules cm^{-3}), but it decreased (p<0.05) to $1.0 \pm 0.2 \times 10^6$ molecules cm^{-3} in the 2016 sampling campaign.

As expected, the formation and loss rates of OH were basically balanced in all the cases. OH was mainly formed from the reaction of HO_2+NO, which accounted for 69.8±1.1% of the total OH production rate over the three sampling campaigns. The photolysis of HONO ranked the second in supplying OH with the contribution of 22.0±1.4%. As stated in section 2.4.2, the average diurnal cycle of HONO measured at TC in 2011 was adopted in the simulations. To assess the uncertainties, we also calculated the HONO concentrations according to the

measured HONO/NO_x ratios and the NO_x concentrations at TC in the three sampling campaigns (Figure S5). The uncertainties in HONO concentrations and in the contributions of HONO to OH formation and loss rates are discussed in Text S3. The formation of OH from HONO photolysis was most efficient in the early morning, which was explained by the morning peak of HONO concentration, due to the nocturnal heterogeneous formation and the vehicle emissions in morning rush hours. Apart from the two dominant pathways, O_3 photolysis (6.3±0.2%), ozonolysis of unsaturated VOCs (1.5±0.2%) and H_2O_2 photolysis (0.2±0.01%) also made some contributions to the formation of OH, with the highest rates at noon or in the early afternoon when the productions of O_3 and H_2O_2 were the most intensive. To sum up, the total formation rates of OH from the primary sources (photolysis of HONO, O_3 and H_2O_2, and ozonolysis of VOCs) were lower than the recycling rates of OH (HO_2+NO) throughout the day at TC, consistent with the results in Xue et al. (2016) simulated at the same site. The dominant role of HO_2+NO in OH formation at TC (average contribution of 69.8±1.1%) might be related to the abundant NO at this site. The same pathway was simulated and accounted for only 42.7±0.2% of the total OH formation rate at an island more than 40 km away from Hong Kong with very low NO concentrations, *i.e.* maximum of 0.56 ppbv (Wang et al., 2018a).

OH was mainly depleted by the reactions with VOCs (32.3±1.2%), NO_2 (31.9±0.9%), CO (19.3±0.6%) and NO (16.5±1.1%). The reaction rates of OH+NO (formation rates of HONO) had the highest values in the morning, approximately in line with the diurnal pattern of the HONO photolysis rates, which however were not completely balanced due to the constraint of HONO to observations in the model. The average net photolysis rates of HONO (differences between the HONO photolysis and formation rates) were $0.68\pm0.21\times10^6$, $0.70\pm0.12\times10^6$ and $0.87\pm0.12\times10^6$ molecules cm^{-3} s^{-1} in the 2007, 2013 and 2016 sampling campaigns, respectively. The losses of OH through the other pathways all exhibited the

highest efficiencies at noon or in the early afternoon. It should be noted that the reaction between OH and NO_2 was not only the sink of OH but also a termination reaction in the photochemical system. In comparison, the termination reaction rates were lower than the OH formation rates from the primary sources (photolysis of HONO, O_3 and H_2O_2, and ozonolysis of VOCs) in the morning (7:00 – 10:00 LT), which were reversed in the following hours of the day due to the increases in OH concentrations.

Consistent with the variations of the local O_3 production, both the local formation and loss rates of OH decreased through 2007 to 2016 (p<0.05), with much more obvious reductions in the later phase (2013-2016). On one hand, the continuous reduction of VOCs resulted in lower HO_2 and RO_2 concentrations (Figure S6), hence the lower production rate of OH through the reaction of HO_2+NO. At the same time, the destruction rates of OH also decreased due to the reductions of OH and the O_3 precursors, except for CO (Figure 7 and Table 1). The decreases of the OH production and destruction rates indicated that the propagation of the reaction cycles, namely the recycling of OH, became slower from 2007 to 2016. This also explained why the locally produced O_3 decreased in these ten years, since O_3 is formed with the consumption and recycling of OH radical.

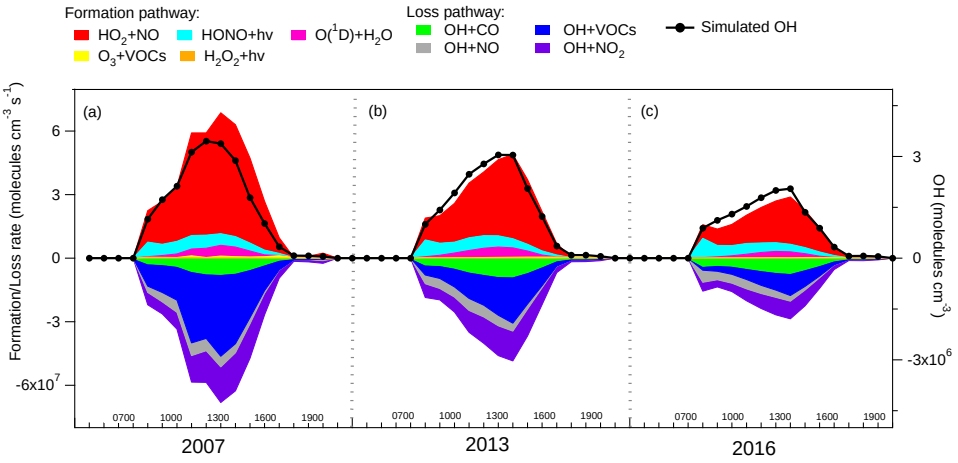

Figure 7. Average diurnal cycles of the OH formation and loss rates during the sampling

periods in (a) 2007, (b) 2013 and (c) 2016.

3.4 Source contributions to the production of O_3 and radicals

3.4.1 Source apportionment

To resolve the sources of O_3 precursors, 27 species, including CO, NO, NO_2, 12 alkanes, 4 alkenes and 8 aromatics, were applied to PMF for source apportionment. These species were either of high abundances or typical tracers of VOC sources in Hong Kong. Source apportionment was conducted for a total of 414 samples covering the three sampling periods, so that the uncertainty of the source apportionment results could be reduced, compared to separate source apportionments for each of the three sampling periods. Figure 8 shows the average profiles of the six sources resolved by PMF. The modelling errors were estimated with the bootstrap method integrated in PMF (Brown et al., 2015).

Factor 1 was assigned as the combination of LPG usage and gasoline evaporation, in view of the high loadings of C_2-C_5 hydrocarbons. Specifically, propane and *i*-/*n*-butanes are the main components of LPG in Hong Kong, and gasoline evaporation generally contains large quantities of *i*-/*n*-pentanes, in particularly *i*-pentane (Guo et al., 2013a; Lyu et al., 2017a). Factor 2 was characterized by moderate to high percentages of *i*-/*n*-pentanes and TEX (toluene, ethylbenzene and xylenes). These species are commonly seen in gasoline exhausts. Therefore, we defined this factor as gasoline exhausts. Both the third and fourth factors indicated solvent-related emissions. While Factor 3 likely represented household solvent usage, due to the dominance of hexane and hexane isomer (3-methylpentane) (Ling and Guo, 2014; Ou et al., 2015), Factor 4 was more related to emissions from coatings and paints, in view of the dominance of the aromatics (Ling and Guo, 2014). Factor 5 was distinguished by the high concentrations of ethane, ethene, ethyne and benzene, together with the relatively heavy (C_7-C_{10}) alkanes, which are typical species in diesel exhausts (Schauer et al., 1999; Kashdan et al., 2008; Sahoo et al., 2011). Therefore, this factor was designated as diesel

exhausts. The last factor denoted for biogenic emissions (BVOCs), due to the exclusive dominance of isoprene (Guenther, 2006).

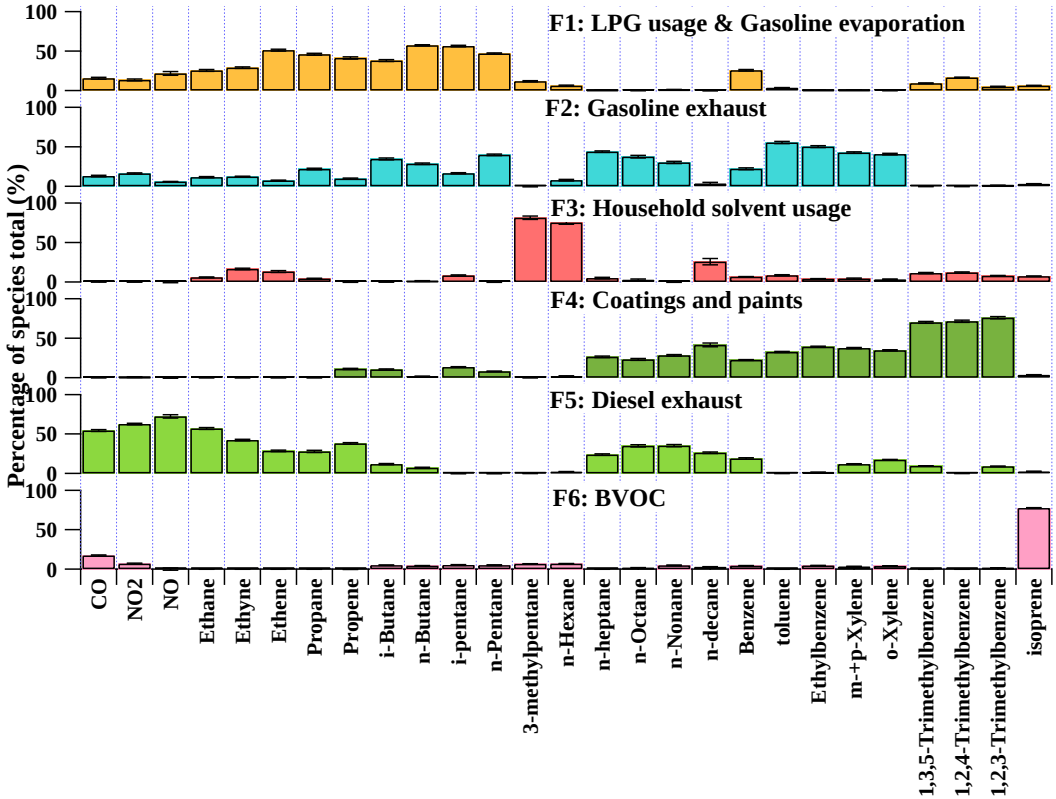

Figure 8. Average profiles of the O_3 precursors sources at TC in the three sampling campaigns. The uncertainties were estimated with the bootstrap method in PMF.

Figure S7 presents the total mixing ratio of VOCs emitted from each individual source extracted from PMF during the three sampling periods in Hong Kong. The VOC emissions from LPG usage and gasoline evaporation decreased significantly (p<0.05) at a rate of -2.61±0.03 ppbv yr^{-1} from 2007 to 2016. However, the VOCs in association with gasoline exhausts experienced an increase (rate = 1.32±0.02 ppbv yr^{-1}, p<0.05) in these years, indicating that the reduction of VOC emissions from LPG usage and gasoline evaporation was not attributable to the change in emissions of gasoline-fuelled vehicles. Insight into the mixing ratios of propane and *i*-/*n*-butanes (LPG tracers) in this source revealed a significant decline from 3.51±0.52 ppbv in the 2007 sampling campaign to 1.27±0.11 ppbv in the 2016

616 sampling campaign. Therefore, the reduction of VOC emissions from LPG usage was most
617 likely the reason of the decrease of VOCs allocated to the source of LPG usage and gasoline
618 evaporation. In fact, it was confirmed by our previous studies (Lyu et al., 2016b; Yao et al.,
619 2019) that the replacement of catalytic converters on LPG-fuelled vehicles during September
620 2013-May 2014 effectively reduced the VOC emissions from LPG-fuelled vehicles in Hong
621 Kong. In addition, the variations in LPG usage in inland PRD, where LPG was extensively
622 used as vehicular and domestic fuels (Liu et al., 2008), might also contribute to the emission
623 reduction of VOCs, in view of the decrease of LPG tracers in this source from 2007
624 (3.51±0.52 ppbv) to 2013 (2.04±0.27 ppbv), when no control was performed against LPG
625 fuelled vehicle emissions in Hong Kong. The VOCs emitted from solvent usage (including
626 the household solvent, coatings and paints) also decreased significantly (p<0.05) from 2007
627 to 2016, likely benefiting from the actions taken to restrict the VOC contents in solvent
628 products starting from 2007 (phase I) and 2010 (phase II) in Hong Kong (Lyu et al., 2017a).
629 VOCs attributable to diesel exhausts decreased (p<0.05) from the 2007 (2.6±0.3 ppbv) to
630 2013 sampling campaign (2.0±0.2 ppbv), which however were unchanged between 2013 and
631 2016 (2.2±0.2 ppbv). In fact, a subsidy program has been implemented in Hong Kong since
632 2007 to progressively eliminate the pre-Euro IV diesel vehicles or to upgrade their emission
633 standards to Euro IV (HKEPD, 2017b), and the effectiveness of this program in VOC
634 reductions till 2013 was confirmed by Lyu et al. (2017a) with the online measurement data at
635 the same site. However, while the phase III of this program (2014-2019) is still ongoing, the
636 VOCs emitted from diesel vehicles remained stable between the 2013 and 2016 sampling
637 campaigns. This undesirable result might be due to the fact that the actions were mainly
638 targeted at the pre-Euro, Euro I and Euro II diesel vehicles before 2013, whereas the phase III
639 of the program initiated in 2014 focused on the Euro III vehicles (HKEPD, 2017b, 2018).
640 Since the former were vehicles with higher emissions, it is not unreasonable that reduction of

VOCs was more discernible between 2007 and 2013. Further, the effectiveness of the phase III program might be somewhat offset by the wearing-out of the pre-existing vehicles and the increase of diesel vehicle populations (Competition Commission, 2017). Further evaluation with more data in a longer period is recommended. At last, the increase of BVOCs from 2007 to 2013 but comparable levels between 2013 and 2016 seemed to be related to the lower (p<0.05) temperature in the 2007 sampling campaign (Figure S8 and Table S6). Besides, the more frequent (62.8%) southeast winds from SCS with higher wind speeds (2.3±0.2 m s^{-1}) might dilute BVOCs emitted from the terrestrial plants in the 2007 sampling campaign.

3.4.2 Source contributions to O_3 production

Figure 9 presents the contributions of VOCs emitted from individual sources to the production and destruction rates of O_3, as well as the simulated contributions to the O_3 mixing ratios. NO_x was not included in these analyses, because of its relatively high uncertainties in source apportionment results due to the short lifetimes. Consistent with the O_3 production and destruction in the whole air, the pathway of HO_2+NO dominated over the reactions between RO_2 and NO in O_3 production for all the individual sources. The destruction of O_3 was mainly driven by NO_2 reacting with OH. For the net O_3 production rate, VOCs attributable to the coatings and paints made the largest contribution (0.38±0.05 ppbv h^{-1}), followed by gasoline exhausts (0.22±0.03ppbv h^{-1}), LPG and gasoline evaporation (0.21±0.03ppbv h^{-1}), BVOCs (0.19±0.03ppbv h^{-1}), household solvent usage (0.15±0.04 ppbv h^{-1}) and diesel exhausts (0.13±0.01ppbv h^{-1}). Despite some peak shifts for the reasons illustrated in section 3.3.1, the O_3 mixing ratios elevated by the individual sources followed the same pattern as the net O_3 production rates, with the highest O_3 enhancement (1.92±0.21 ppbv) by the source of coatings and paints and the lowest increase by household solvent usage (0.86±0.06 ppbv) and diesel exhausts (0.83±0.06 ppbv). The contributions of source-specific VOCs to O_3 production, particularly the importance of solvent usage in O_3 formation

in Hong Kong, were generally in line with previous studies (Ling and Guo, 2014; Ou et al., 2015). This was actually expected according to the reactivity of major VOCs in each source. For example, the TEX in the source of coatings and paints (Figure 8) have been identified to be of high O_3 formation potentials (Lau et al., 2010; Ling et al., 2011, 2013). However, the PBM-MCM model simulations enabled us to quantitatively evaluate the contributions of VOC sources to O_3 production rates.

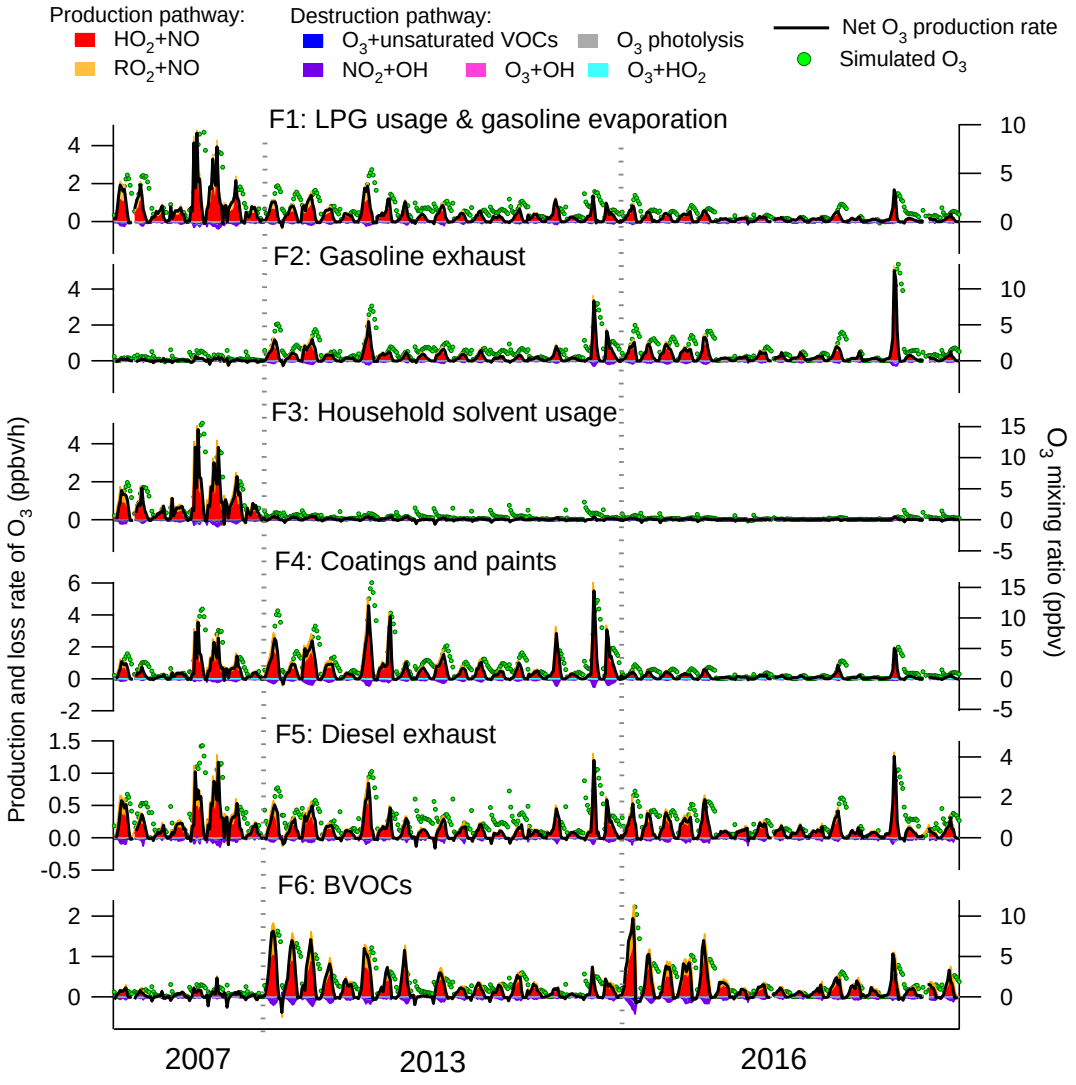

Figure 9. Contributions of VOCs in individual sources to the production and destruction rates of O_3 and to the O_3 mixing ratios in the three sampling campaigns.

From a historical perspective, we found that the contribution of LPG usage and gasoline evaporation to O_3 production significantly decreased (p<0.05) from 2007 to 2016 sampling campaign (2007: 0.51±0.11 ppbv h^{-1}; 2013: 0.20±0.03 ppbv h^{-1}; 2016: 0.10±0.02 ppbv h^{-1}), which coincided with the variations of VOCs emitted from LPG-fuelled vehicles as discussed above. Gasoline exhaust contributed much less (p<0.05) to the net O_3 production rate in 2007 (0.02±0.01ppbv h^{-1}), than those in 2013 (0.26±0.05ppbv h^{-1}) and 2016 (0.27±0.07ppbv h^{-1}), in line with the variations of VOCs emitted from this source. The reductions of VOC emissions from solvents also resulted in the consistent decrease of the net O_3 production rate from 1.22±0.17 ppbv h^{-1} in the 2007 to 0.14±0.05 ppbv h^{-1} in the 2016 sampling campaign. The O_3 production rates contributed by VOCs in diesel exhausts were reduced from 2007 (0.21±0.05 ppbv h^{-1}) to 2013 (0.11±0.02 ppbv h^{-1}) and remained unchanged thereafter (2016: 0.11±0.02 ppbv/h). The O_3 production rate traceable to BVOCs showed a significant increase from 2007 (0.04±0.02 ppbv h^{-1}) to 2016 (0.22±0.04 ppbv h^{-1}), since the mixing ratios of BVOCs significantly increased (p<0.05) in these years. It is noteworthy that the changes in meteorological conditions in these three sampling campaigns might also partially account for the variations in the source contributions to O_3 production. For example, the 2013 sampling campaign was characterized by the relatively higher temperature and lowest relative humidity among the three sampling periods, which favoured O_3 formation in 2013 (Table S6). Besides, due to limited samples in this study, we recommend further assessments with more data in longer periods to be carried out in future study.

4 Conclusions

Photochemical pollution with high and increasing concentrations of O_3 has been an important environmental issue in South China. With the observation data of O_3 and its precursors at a suburban site in Hong Kong, downwind of South China, this study analysed the inter-annual variations of O_3 and its photochemistry, as well as the contributions of VOC sources to the

local O_3 production rates in 2007, 2013 and 2016. To our knowledge, this is the first time that a substantial alleviation of O_3 pollution in this region was identified between 2013 and 2016, in contrast to the repeatedly confirmed O_3 increase before 2013. In addition to the changes in meteorological conditions among the three sampling campaigns, the termination of the rise in regionally transported O_3 and the decrease of the local O_3 production rate contributed to the decline of O_3 in the later period. The emission reductions (particularly for NO_x) in mainland China starting from 2013, the year when the China's Clean Air Action Plan was launched, might more or less play a role in ceasing the increase of regional O_3. In Hong Kong, the replacement of catalytic converters and the constraints of VOC contents in solvent products led to the reductions of VOC emissions from LPG-fuelled vehicles and solvent usage, respectively. As a result, the local O_3 production rate and the recycling rate of OH radical decreased substantially from 2013 to 2016. Though the variations in meteorological conditions and the limited sample size might somewhat introduce uncertainties to the conclusions drawn from the present study, it is plausible that the local and regional interventions were effective on the control of O_3 pollution in Hong Kong. Nevertheless, studies with more data in longer periods should be conducted, not only in Hong Kong but also in mainland China where O_3 is still increasing in most of the territories.

Author contribution

Hai Guo and Fei Jiang initiated and designed the experiments, and Xufei Liu and Xiaopu Lyu carried them out. Xiaopu Lyu and Yu Wang developed the model code and performed the simulations. Xufei Liu and Xiaopu Lyu prepared the manuscript and Hai Guo finalized the manuscript with contributions from all co-authors.

Acknowledgements

This study was supported by the National Key R&D Program of China via grant No. 2017YFC0212001, Research Grants Council of the Hong Kong Special Administrative Region Government via grants PolyU 152052/14E, PolyU 152052/16E and CRF/C5004-15E, the Public Policy Research Funding Scheme from Policy Innovation and Co-ordination Office of the Hong Kong Special Administrative Region Government (Project Number: 2017.A6.094.17D), and the Hong Kong Polytechnic University Ph.D. scholarships via research project #RUDC.

References

Ashmore, M. R.: Assessing the future global impacts of ozone on vegetation, Plant. Cell. Environ., 28, 949-964, 2005.

Bell, M. L., McDermott, A., Zeger, S. L., Samet, J. M., and Dominici, F.: Ozone and short-term mortality in 95 US urban communities, 1987-2000, JAMA, 292, 2372-2378, 2004.

Brown, S. G., Frankel, A., and Hafner, H. R.: Source apportionment of VOCs in the Los Angeles area using positive matrix factorization, Atmos. Environ., 41, 227-237, 2007.

Brown, S. G., Eberly, S., Paatero, P., and Norris, G. A.: Methods for estimating uncertainty in PMF solutions, Sci. Total Environ., 518, 626-635, 2015.

Census and Statistics Department (CSD), 2011 Population Census in Hong Kong, available at: https://www.census2011.gov.hk/en/constituency-area-i.html (last access: 25 October 2018), 2011.

Census and Statistics Department (CSD), District profile for 2016 Population Census in Hong Kong, available at: https://www.bycensus2016.gov.hk/en/bc-dp.html (last access: 25 October 2018), 2018.

Cheng, H. R., Guo, H., Wang, X. M., Saunders, S. M., Lam, S. H. M., Jiang, F., Wang, T. J., Ding, A. J., Lee, S. C., and Ho, K. F.: On the relationship between ozone and its precursors in

747 the Pearl River Delta: application of an observation-based model (OBM), Environ. Sci. Pollut.
748 Res., 17, 547-560, 2010.
749 Cheng, H. R., Saunders, S. M., Guo, H., Louie, P. K. K., and Jiang, F.: Photochemical
750 trajectory modeling of ozone concentrations in Hong Kong, Environ. Pollut, 180, 101-110,
751 2013.
752 Cheng, Y., Lee, S. C., Huang, Y., Ho, K. F., Ho, S. S. H., Yau, P. S., Louie, P. K. K., and
753 Zhang, R. J.: Diurnal and seasonal trends of carbonyl compounds in roadside, urban, and
754 suburban environment of Hong Kong, Atmos. Environ., 89, 43-51, 2014.
755 Chou, C. C. K, Liu, S. C., Lin, C. Y., Shiu, C. J., and Chang, K. H.: The trend of surface
756 ozone in Taipei, Taiwan, and its causes: Implications for ozone control strategies, Atmos.
757 Environ., 40, 3898-3908, 2006.
758 Colman, J. J., Swanson, A. L., Meinardi, S., Sive, B. C., Blake, D. R., and Rowland, F. S.:
759 Description of the analysis of a wide range of volatile organic compounds in whole air
760 samples collected during PEM-Tropics A and B, Anal. Chem., 73, 3723-3731, 2001.
761 Competition Commission: Report on Study into Hong Kong's Auto-fuel Market, available at:
762 https://www.compcomm.hk/en/media/press/files/Full_Report_Auto_fuel_Market_Study_Rep
763 ort_Eng.pdf (last access: 25 October 2018), 2017.
764 Cui, J., Pandey Deolal, S., Sprenger, M., Henne, S., Staehelin, J., Steinbacher, M., and
765 Nédélec, P.: Free tropospheric ozone changes over Europe as observed at Jungfraujoch
766 (1990–2008): An analysis based on backward trajectories, J. Geophys. Res. Atmos., 116,
767 D10304, https://doi.org/10.1029/2010JD015154, 2011.
768 Cui, L., Zhang, Z., Huang, Y., Lee, S. C., Blake, D. R., Ho, K. F., Wang, B., Gao, Y., Wang,
769 X. M., and Louie, P. K. K. Measuring OVOCs and VOCs by PTR-MS in an urban roadside
770 microenvironment of Hong Kong: relative humidity and temperature dependence, and field
771 inter-comparisons, Atmos. Meas. Tech., 9, 5763-5779, 2016.

772 Derwent, R. G., Manning, A. J., Simmonds, P. G., Spain, T. G., and O'Doherty, S.: Analysis
773 and interpretation of 25 years of ozone observations at the Mace Head Atmospheric Research
774 Station on the Atlantic Ocean coast of Ireland from 1987 to 2012, Atmos. Environ., 80, 361-
775 368, 2013.
776 Ding, A. J., Wang, T., Zhao, M., Wang, T. J., and Li, Z. K.: Simulation of sea-land breezes
777 and a discussion of their implications on the transport of air pollution during a multi-day
778 ozone episode in the Pearl River Delta of China, Atmos. Environ., 38, 6737-6750, 2004.
779 Ding, A.J., Wang, T., Thouret, V., Cammas, J., and Nédélec, P.: Tropospheric ozone
780 climatology over Beijing: analysis of aircraft data from the MOZAIC program, Atmos. Chem.
781 Phys., 8, 1-13, 2008.
782 Dongguan Environment Protection Department (DGEPD), Clean air action plan in Pearl
783 River Delta region, Phase II (2013-2015), available at: http://dgepb.dg.gov.cn
784 /publicfiles///business/htmlfiles/dgepb/cmsmedia/document/doc172679.pdf (last access: 25
785 October 2018), 2013.
786 Guenther, A., Karl, T., Harley, P., Wiedinmyer, C., Palmer, P.I., and Geron, C.: Estimates of
787 global terrestrial isoprene emissions using MEGAN (Model of Emissions of Gases and
788 Aerosols from Nature), Atmos. Chem. Phys., 6, 3181-3210, 2006.
789 George, I. J., Matthews, P. S. J., Whalley, L. K., Brooks, B., Goddard, A., Baeza-Romero, M.
790 T., and Heard, D. E.: Measurements of uptake coefficients for heterogeneous loss of HO_2
791 onto submicron inorganic salt aerosols, Phys. Chem. Chem. Phys., 15, 12829-12845, 2013.
792 Guo, H., Jiang, F., Cheng, H. R., Simpson, I. J., Wang, X. M., Ding, A. J., Wang, T. J.,
793 Saunders, S. M., Wang, T., Lam, S. H. M., Blake, D. R., Zhang, Y. L., and Xie, M.:
794 Concurrent observations of air pollutants at two sites in the Pearl River Delta and the
795 implication of regional transport, Atmos. Chem. Phys., 9, 7343-7360, 2009.

796 Guo, H., Cheng, H. R., Ling, Z. H., Louie, P. K. K., and Ayoko, G. A.: Which emission
797 sources are responsible for the volatile organic compounds in the atmosphere of Pearl River
798 Delta? J. Hazard. Mater., 188, 116-124, 2011.
799 Guo, H., Ling, Z. H., Cheung, K., Jiang, F., Wang, D. W., Simpson, I. J., Barletta, B.,
800 Meinardi, S., Wang, T. J., Wang, X. M., Saunders, S. M., and Blake, D. R.: Characterization
801 of photochemical pollution at different elevations in mountainous areas in Hong Kong,
802 Atmos. Chem. Phys., 13, 3881-3898, 2013a.
803 Guo, H., Ling, Z. H., Cheung, K., Wang, D. W., Simpson, I. J., and Blake, D. R.: Acetone in
804 the atmosphere of Hong Kong: Abundance, sources and photochemical precursors, Atmos.
805 Environ., 65, 80-88, 2013b.
806 Guo, H., Ling, Z. H., Cheng, H. R., Simpson, I. J., Lyu, X. P., Wang, X. M., Shao, M., Lu, H.
807 X., Ayoko, G., Zhang, Y. L. and Saunders, S. M.: Tropospheric volatile organic compounds
808 in China, Sci. Total Environ., 574, 1021-1043, 2017.
809 Hong Kong Environmental Protection Department (HKEPD): Inquire and Download Air
810 Quality Monitoring Data, available at: epic.epd.gov.hk/ca/uid/airdata (last access: 25 October
811 2018), 2017a.
812 Hong Kong Environmental Protection Department (HKEPD): Cleaning the Air at Street
813 Level, available at: http://www.epd.gov.hk/epd/english/environmentinhk/air/prob_solutions
814 /strategies_apc.html (last access: 25 October 2018), 2017b.
815 Hong Kong Environmental Protection Department (HKEPD): Phasing Out Pre-Euro IV
816 Diesel Commercial Vehicles, available at: https://www.epd.gov.hk/epd/english
817 /environmentinhk/air/prob_solutions/Phasing_out_diesel_comm_veh.html (last access: 25
818 October 2018), 2018.

819 Hong Kong Observatory (HKO): Real-time Data Display from ENVF Atmospheric &
820 Environmental Database, available at: http://envf.ust.hk/dataview/hko_wc/current/ (last
821 access: 25 October 2018), 2017.
822 Huang, J. P., Fung, J. C., Lau, A. K., and Qin, Y.: Numerical simulation and process analysis
823 of typhoon-related ozone episodes in Hong Kong, J. Geophys. Res. Atmos., 110, D05301,
824 https://doi.org/10.1029/2004jd004914, 2005.
825 Jacob, D. J.: Introduction to atmospheric chemistry, Princeton University Press, Princeton,
826 New Jersey, 1999.
827 Jenkin, M. E., Saunders, S. M., and Pilling, M. J.: The tropospheric degradation of volatile
828 organic compounds: a protocol for mechanism development, Atmos. Environ., 31, 81-104,
829 1997.
830 Jenkin, M. E., Saunders, S. M., Wagner, V., and Pilling, M. J.: Protocol for the development
831 of the Master Chemical Mechanism, MCM v3 (Part B): tropospheric degradation of aromatic
832 volatile organic compounds, Atmos. Chem. Phys., 3, 181-193, 2003.
833 Jiang, F., Guo, H., Wang, T. J., Cheng, H. R., Wang, X. M., Simpson, I. J., Ding, A. J.,
834 Saunders, S. M., Lam, S. H. M., and Blake, D. R.: An ozone episode in the Pearl River Delta:
835 Field observation and model simulation, J. Geophys. Res., 115, D22305,
836 https://doi.org/10.1029/2009JD013583, 2010.
837 Jiang, Y. C., Zhao, T. L., Liu, J., Xu, X. D., Tan, C. H., Cheng, X. H., Bi, X. Y., Gan, J. B.,
838 You, J. F., and Zhao, S. Z.: Why does surface ozone peak before a typhoon landing in
839 southeast China? Atmos. Chem. Phys., 15, 13331-13338, 2015.
840 Johnson, B.T.: Diesel engine emissions and their control, Platin. Met. Rev., 52, 23-37, 2008.
841 Kanaya, Y., Pochanart, P., Liu, Y., Li, J., Tanimoto, H., Kato, S., Suthawaree, J., Inomata, S.,
842 Taketani, F., Okuzawa, K., and Kawamura, K.: Rates and regimes of photochemical ozone

production over Central East China in June 2006: a box model analysis using comprehensive measurements of ozone precursors, Atmos. Chem. Phys., 9, 7711-7723, 2009.

Kashdan, J.T.: Tracer LIF Visualisation Studies of Piston-Top Fuel Films in a Wall-Guided, Low-NO_x Diesel Engine, SAE Tech. Paper, 2008-01-2474, 2008.

Lakey, P. S. J., George, I. J., Whalley, L. K., Baeza-Romero, M. T., and Heard, D. E.: Measurements of the HO_2 uptake coefficients onto single component organic aerosols, Environ. Sci. Technol., 49, 4878-4885, 2015.

Lam, K. S., Wang, T. J., Wu, C. L., and Li, Y. S.: Study on an ozone episode in hot season in Hong Kong and transboundary air pollution over Pearl River Delta region of China, Atmos. Environ., 39, 1967-1977, 2005.

Lam, S. H. M., Saunders, S. M., Guo, H., Ling, Z. H., Jiang, F., Wang, X. M., and Wang, T. J.: Modelling VOC source impacts on high ozone episode days observed at a mountain summit in Hong Kong under the influence of mountain-valley breezes, Atmos. Environ., 81, 166-176, 2013.

Lau, A. K. H., Yuan, Z., Yu, J. Z., and Louie, P. K.: Source apportionment of ambient volatile organic compounds in Hong Kong, Sci. Total Environ., 408, 4138-4149, 2010.

Lee, E., Chan, C. K., and Paatero, P.: Application of positive matrix factorization in source apportionment of particulate pollutants in Hong Kong, Atmos. Environ., 33, 3201-3212, 1999.

Lefohn, A. S., Shadwick, D. and Oltmans, S. J.: Characterizing changes in surface ozone levels in metropolitan and rural areas in the United States for 1980–2008 and 1994–2008, Atmos. Environ., 44, 5199-5210, 2010.

Li, K., Jacob, D. J., Liao, H., Shen, L., Zhang, Q., and Bates, K. H.: Anthropogenic drivers of 2013–2017 trends in summer surface ozone in China, Proc. Natl. Acad. Sci. U. S. A., 116, 2, 422-427, 2019.

867 Lin, M., Horowitz, L.W., Payton, R., Fiore, A. M., and Tonnesen, G.: US surface ozone
868 trends and extremes from 1980 to 2014: quantifying the roles of rising Asian emissions,
869 domestic controls, wildfires, and climate, Atmos. Chem. Phys., 17, 2943-2970, 2017.
870 Ling, Z. H. and Guo, H.: Contribution of VOC sources to photochemical ozone formation
871 and its control policy implication in Hong Kong, Environ. Sci. Policy, 38, 180-191, 2014.
872 Ling, Z. H., Guo, H., Cheng, H. R., and Yu, Y. F.: Sources of ambient volatile organic
873 compounds and their contributions to photochemical ozone formation at a site in the Pearl
874 River Delta, southern China, Environ. Pollut., 159, 2310-2319, 2011.
875 Ling, Z. H., Guo, H., Zheng, J. Y., Louie, P. K. K., Cheng, H. R., Jiang, F., Cheung, K.,
876 Wong, L. C., and Feng, X. Q.: Establishing a conceptual model for photochemical ozone
877 pollution in subtropical Hong Kong, Atmos. Environ., 76, 208–220, 2013.
878 Ling, Z. H., Guo, H., Lam, S. H. M., Saunders, S. M., and Wang, T.: Atmospheric
879 photochemical reactivity and ozone production at two sites in Hong Kong: Application of a
880 Master Chemical Mechanism-photochemical box model, J. Geophys. Res. Atmos., 119,
881 10567-10582, 2014.
882 Ling, Z., Guo, H., Simpson, I. J., Saunders, S. M., Lam, S. H. M., Lyu, X., and Blake, D. R.:
883 New insight into the spatiotemporal variability and source apportionments of C_1–C_4 alkyl
884 nitrates in Hong Kong, Atmos. Chem. Phys., 16, 8141-8156, 2016a.
885 Ling, Z., Guo, H., Chen, G., Lam, S. H. M., and Fan, S.: Formaldehyde and acetaldehyde at
886 different elevations in mountainous areas in Hong Kong, Aerosol Air Qual. Res., 16, 1868-
887 1878, 2016b.
888 Liu, Y., Shao, M., Lu, S. H., Chang, C. C., Wang, J. L., and Chen, G.: Volatile Organic
889 Compound (VOC) measurements in the Pearl River Delta (PRD) region, China, Atmos.
890 Chem. Phys., 8, 1531-1545, 2008.

Liu, Z., Wang, Y., Gu, D., Zhao, C., Huey, L. G., Stickel, R., Liao, J., Shao, M., Zhu, T., Zeng, L., and Amoroso, A.: Summertime photochemistry during CAREBeijing-2007: RO_x budgets and O_3 formation, Atmos. Chem. Phys., 12, 7737-7752, 2012.

Lyu, X. P., Ling, Z. H., Guo, H., Saunders, S. M., Lam, S. H. M., Wang, N., Wang, Y., Liu, M., and Wang, T.: Re-examination of C_1-C_5 alkyl nitrates in Hong Kong using an observation-based model, Atmos. Environ., 120, 28-37, 2015.

Lyu, X. P., Liu, M., Guo, H., Ling, Z. H., Wang, Y., Louie, P. K. K., and Luk, C. W. Y.: Spatiotemporal variation of ozone precursors and ozone formation in Hong Kong: grid field measurement and modelling study, Sci. Total Environ., 569, 1341-1349, 2016a.

Lyu, X. P., Guo, H., Simpson, I. J., Meinardi, S., Louie, P. K. K., Ling, Z. H., Wang, Y., Liu, M., Luk, C. W. Y., Wang, N., and Blake, D. R.: Effectiveness of replacing catalytic converters in LPG-fuelled vehicles in Hong Kong, Atmos. Chem. Phys., 16, 6609-6626, 2016b.

Lyu, X. P., Chen, N., Guo, H., Zhang,W. H., Wang, N.,Wang, Y., and Liu, M.: Ambient volatile organic compounds and their effect on ozone production in Wuhan, Central China, Sci. Total Environ., 541, 200-209, 2016c.

Lyu, X. P., Zeng, L. W., Guo, H., Simpson, I. J., Ling, Z. H., Wang, Y., Murray, F., Louie, P. K. K., Saunders, S. M., Lam, S. H. M., and Blake, D. R.: Evaluation of the effectiveness of air pollution control measure in Hong Kong, Environ. Pollut., 220, 87-94, 2017a.

Lyu, X. P., Guo, H., Wang, N., Simpson, I. J., Cheng, H. R., Zeng, L. W., Saunders, S. M., Lam, S. H. M., Meinardi, S., and Blake, D. R.: Modeling C_1-C_4 alkyl nitrate photochemistry and their impacts on O_3 production in urban and suburban environments of Hong Kong, J. Geophys. Res. Atmos., 122, 10539-10556, 2017b.

Madronich, S. and Flocke, S.: The role of solar radiation in atmospheric chemistry, Environ. Photochem., 1-26, 1999.

916 Ministry of Ecology and Environment of the People's Republic of China (MEE PRC): Action
917 plan for preventing and controlling air pollution in Guangdong Province, China, available at:
918 http://www.mee.gov.cn/xxgk/hjyw/201403/t20140303_268619.shtml (last access: 25 October
919 2018), 2014.
920 NARSTO: An Assessment of tropospheric ozone pollution: a North American perspective,
921 NARSTO synthesis team, available at: http://cdiac.ess-dive.lbl.gov
922 /programs/NARSTO/ozone_assessment.html (last access: 25 October 2018), 2000.
923 National Research Council (NRC): Rethinking the ozone problem in urban and regional air
924 pollution, National Academies Press, 1992.
925 Norris, G., Wade, K., and Foley, C.: EPA Positive Matrix Factorization (PMF) 3.0
926 Fundamentals & User Guide, EPA 600/R-08/108, US Environmental Protection Agency,
927 Office of Research and Development, Washington, 2008.
928 Norris, G., Duvall, R., Brown, S., and Song, B.: EPA Positive Matrix Factorization (PMF)
929 5.0 Fundamentals & User Guide, EPA 600/R-14/108, US Environmental Protection Agency,
930 Office of Research and Development, Washington, 2014.
931 Ou, J.M., Guo, H., Zheng, J.Y., Cheung, K., Louie, P.K.K., Ling, Z.H., and Wang, D.W.:
932 Concentrations and sources of non-methane hydrocarbons (NMHCs) from 2005 to 2013 in
933 Hong Kong: A multi-year real-time data analysis. Atmos. Environ., 103, 196-206, 2015.
934 Paatero, P.: Least squares formulation of robust non-negative factor analysis, Chemometr.
935 Intell. Lab., 37, 23-35, 1997.
936 Paatero, P.: User's Guide for Positive Matrix Factorization Programs PMF2 and PMF3, Part
937 1: Tutorial, Prepared by University of Helsinki, Finland (February), 2000a.
938 Paatero, P.: User's Guide for Positive Matrix Factorization Programs PMF2 and PMF3, Part
939 2: Reference, Prepared by University of Helsinki, Finland, 2000b.

940 Parrish, D. D., Lamarque, J. F., Naik, V., Horowitz, L., Shindell, D. T., Staehelin, J., Derwent,
941 R., Cooper, O. R., Tanimoto, H., Volz-Thomas, A., and Gilge, S.: Long-term changes in
942 lower tropospheric baseline ozone concentrations: Comparing chemistry-climate models and
943 observations at northern midlatitudes., J. Geophys. Res. Atmos., 119, 5719-5736, 2014.
944 Polissar, A. V., Hopke, P. K., Paatero, P., Malm, W. C., and Sisler, J. F.: Atmospheric aerosol
945 over Alaska: 2. Elemental composition and sources, J. Geophys. Res. Atmos., 103, D15,
946 19045-19057, 1998.
947 Reff, A., Eberly, S. I., and Bhave, P. V.: Receptor modeling of ambient particulate matter
948 data using positive matrix factorization: review of existing methods, J. Air Waste Manag.
949 Assoc., 57, 146-154, 2007.
950 Richter, A., Burrows, J.P. Nub, H., Granier, C., and Niemeier, U.: Increase in tropospheric
951 nitrogen dioxide over China observed from space, Nature, 437, 129, 2005.
952 Sahoo, D., Petersen, B., and Miles, P.: Measurement of equivalence ratio in a light-duty low
953 temperature combustion diesel engine by planar laser induced fluorescence of a fuel tracer,
954 SAE Int. J. Engines, 4, 2312-2325, 2011.
955 Saunders, S. M., Jenkin, M. E., Derwent, R. G., and Pilling, M. J.: Protocol for the
956 development of the Master Chemical Mechanism, MCM v3 (Part A): tropospheric
957 degradation of non-aromatic volatile organic compounds, Atmos. Chem. Phys., 3, 161-180,
958 2003.
959 Schauer, J. J., Kleeman, M. J., Cass, G. R., and Simoneit, B. R.: Measurement of emissions
960 from air pollution sources. 2. C_1 through C_{30} organic compounds from medium duty diesel
961 trucks, Environ. Sci. Technol., 33, 1578-1587, 1999.
962 Sillman, S.: The relation between ozone, NO_x and hydrocarbons in urban and polluted rural
963 environments, Atmos. Environ., 33, 1821-1845, 1999.

964 Simpson, I. J., Blake, N. J., Barletta, B., Diskin, G. S., Fuelberg, H. E., Gorham, K., Huey, L.
965 G., Meinardi, S., Rowland, F. S., Vay, S. A., Weinheimer, A. J., Yang, M., and Blake, D. R.:
966 Characterization of trace gases measured over Alberta oil sands mining operations: 76
967 speciated C_2-C_{10} volatile organic compounds (VOCs), CO_2, CH_4, CO, NO, NO_2, NO_y, O_3 and
968 SO_2, Atmos. Chem. Phys., 10, 11931−11954, 2010.
969 So, K. L. and Wang, T.: On the local and regional influence on ground-level ozone
970 concentrations in Hong Kong, Environ. Pollut., 123, 307-317, 2003.
971 United States Environmental Protection Agency (US EPA): Positive Matrix Factorization
972 Model for environmental data analyses, available at https://www.epa.gov/air-
973 research/positive-matrix-factorization-model-environmental-data-analyses (last access: 25
974 October 2018), 2017.
975 Wang, H., Lyu, X. P., Guo, H., Wang, Y., Zou, S. C., Ling, Z. H., Wang, X. M., Jiang, F.,
976 Zeren, Y. Z., Pan, W. Z., Huang X. B., and Shen, J.: Ozone pollution around a coastal region
977 of South China Sea: Interaction between marine and continental air, Atmos. Chem. Phys., 18,
978 4277-4295, 2018b.
979 Wang, H. X., Kiang, C. S., Tang, X. Y., Zhou, X. J., and Chameides, W. L.: Surface ozone:
980 A likely threat to crops in Yangtze delta of China, Atmos. Environ., 39, 3843-3850, 2005.
981 Wang, N., Guo, H., Jiang, F., Ling, Z. H., and Wang, T.: Simulation of ozone formation at
982 different elevations in mountainous area of Hong Kong using WRF-CMAQ model, Sci. Total
983 Environ, 505, 939-951, 2015.
984 Wang, T., Wei, X. L., Ding, A. J., Poon, S. C., Lam, K. S., Li, Y. S., Chan, L. Y., and Anson,
985 M.: Increasing surface ozone concentrations in the background atmosphere of Southern China,
986 1994-2007, Atmos. Chem. Phys., 9, 6217-6227, 2009.

Wang, T., Xue, L. K., Brimblecombe, P., Lam, Y. F., Li, L., and Zhang, L.: Ozone pollution in China: A review of concentrations, meteorological influences, chemical precursors, and effects, Sci. Total Environ., 575, 1582-1596, 2017b.

Wang, Y., Wang, H., Guo, H., Lyu, X. P., Cheng, H. R., Ling, Z. L., Louie, P. K. K., Simpson, I J., Meinardi, S., and Blake, D. R.: Long-term O_3- precursor relationships in Hong Kong: field observation and model simulation, Atmos. Chem. Phys., 17, 10919-10935, 2017a.

Wang, Y., Guo, H., Zou, S. C., Lyu, X. P., Ling, Z. H., Cheng, H. R., and Zeren, Y. Z.: Surface O_3 photochemistry over the South China Sea: Application of a near-explicit chemical mechanism box model, Environ. Pollut., 234, 155-166, 2018a.

Willmott, C. J.: Some comments on the evaluation of model performance., B. Am. Meteorol. Soc., 63, 1309-1313, 1982.

Xu, X., Lin, W., Wang, T., Yan, P., Wang, J., Meng, Z., and Wang, Y.: Long-term trend of surface ozone at a regional background station in eastern China 1991-2006: enhanced variability, Atmos. Chem. Phys., 8, 2595-2607, 2008.

Xu, Z., Wang, T., Wu, J., Xue, L., Chan, J., Zha, Q., Zhou, S., Louie, P. K., and Luk, C. W.: Nitrous acid (HONO) in a polluted subtropical atmosphere: Seasonal variability, direct vehicle emissions and heterogeneous production at ground surface, Atmos. Environ., 106, 100-109, 2015.

Xue, L. K., Wang, T., Louie, P. K., Luk, C. W., Blake, D. R., and Xu, Z.: Increasing external effects negate local efforts to control ozone air pollution: a case study of Hong Kong and implications for other Chinese cities, Environ. Sci. Technol., 48, 10769-10775, 2014a.

Xue, L. K., Wang, T., Gao, J., Ding, A. J., Zhou, X. H., Blake, D. R., Wang, X. F., Saunders, S. M., Fan, S. J., Zuo, H. C., and Zhang, Q. Z.: Ground-level ozone in four Chinese cities: precursors, regional transport and heterogeneous processes, Atmos. Chem. Phys., 14, 13175-13188, 2014b.

Xue, L. K., Gu, R. R., Wang, T., Wang, X. F., Saunders, S., Blake, D., Louie, P. K. K., Luk, C. W. Y., Simpson, I., Xu, Z., Wang, Z., Gao, Y., Lee, S. C., Mellouki, A., and Wang, W. X.: Oxidative capacity and radical chemistry in the polluted atmosphere of Hong Kong and Pearl River Delta regional analysis of a severe photochemical smog episode, Atmos. Chem., Phys., 16, 9891-9903, 2016.

Yao, C., Cheung, C. S., Cheng, C., Wang, Y., Chan, T. L., and Lee, S. C.: Effect of diesel/methanol compound combustion on diesel engine combustion and emissions, Energy Convers. Manag., 49, 1696-1704, 2008.

Yao, D., Lyu, X., Murray, F., Morawska, L., Yu, W., Wang, J., and Guo, H.: Continuous effectiveness of replacing catalytic converters on liquified petroleum gas-fueled vehicles in Hong Kong., Sci. Total Environ., 648, 830-838, 2019.

Zeng, L., Lyu, X., Guo, H., Zou, S., and Ling, Z.: Photochemical Formation of C_1–C_5 Alkyl Nitrates in Suburban Hong Kong and over the South China Sea, Environ. Sci. Technol., 52, 5581-5589, 2018.

Zhang, J., Wang, T., Chameides, W. L., Cardelino, C., Kwok, J., Blake, D. R., Ding, A., and So, K. L.: Ozone production and hydrocarbon reactivity in Hong Kong, Southern China, Atmos. Chem. Phys., 7, 557-573, 2007.

Zhang, Y., Wang, X., Blake, D.R., Li, L., Zhang, Z., Wang, S., Guo, H., Lee, S.C., Gao, B., Chan, L., and Wu, D.: Aromatic hydrocarbons as ozone precursors before and after outbreak of the 2008 financial crisis in the Pearl River Delta region, south China., J. Geophys. Res. Atmos., 117, D15306, https://doi.org/10.1029/2011JD017356, 2012.

Zheng, B., Tong, D., Li, M., Liu, F., Hong, C., Geng, G., Li, H., Li, X., Peng, L., Qi, J., and Yan, L.: Trends in China's anthropogenic emissions since 2010 as the consequence of clean air actions., Atmos. Chem. Phys., 18, 14095-14111, 2018.

Supplement for the manuscript "Inter-comparison of O_3 formation and radical chemistry in the past decade at a suburban site in Hong Kong"

Xufei Liu[1,#], Xiaopu Lyu[1,#], Yu Wang[1], Fei Jiang[2], Hai Guo[1,*]

[1] Air Quality Studies, Department of Civil and Environmental Engineering, The Hong Kong Polytechnic University, Hong Kong, China

[2] Jiangsu Provincial Key Laboratory of Geographic Information Science and Technology, International Institute for Earth System Science, Nanjing University, Nanjing, China

*Corresponding author. ceguohai@polyu.edu.hk

# Both authors made equal contribution.

Text S1. Determination of the locally produced and regionally transported O_3 and discussion on the uncertainties.

As an observation based model, PBM-MCM has been widely used to simulate the in-situ O_3 production (Lam et al., 2013; Ling et al., 2014; Lyu et al., 2017b; Wang et al., 2017a). Therefore, the O_3 simulated by PBM-MCM can be regarded as the locally produced O_3, and the differences between the observed and simulated O_3 were taken as the regionally transported O_3. However, it should be noted that the observed concentrations of O_3 precursors could be partially built up by regional transport. For example, under the northwest winds, the average mixing ratios of CO (693.9 ±25.5 ppbv), ethyne (2.15 ±0.22 ppbv), ethane (2.31 ±0.25 ppbv), propane (2.97 ±0.51 ppbv) and toluene (2.42 ±0.52 ppbv) were the highest among all the wind sectors, surpassing their average concentrations under light winds (wind speeds < 2 m/s) by 11.3%, 48.0%, 42.5%, 53.5% and 138.5%, respectively. Since the PBM-MCM was constrained by the observed concentrations of O_3 precursors, the share of regionally transported O_3 precursors in the observations made contributions to the simulated O_3, which in fact represented a kind of regional transport. Therefore, the locally produced O_3 was to some extent overestimated in this way. Conversely, the regionally transported O_3 was underestimated. However, it is difficult to accurately quantify the contributions of regional transport to O_3 precursors at the site. Moreover, due to the non-linear relationships between

O_3 and its precursors, we did not quantitatively evaluate the overestimation of the locally produced O_3 and the underestimation of the regionally transported O_3.

Text S2. Set-up of the simulation scenarios

The base scenario (scenario A) was established to simulate the local production of O_3, with the observed concentrations of air pollutants (excluding O_3) as model inputs. The observed O_3 was not input because the simulated O_3 would be constrained to the observed values with the outputs exactly the same as the inputs otherwise. The scenario B was established to simulate O_3 under the assumption that a source of VOCs was totally removed. Namely, the VOCs emitted from a specific source were subtracted from the observed VOCs when allocating the model inputs. In this study, six sources of VOCs were identified (see section 3.4.1). Therefore, 6 sub-scenarios were included in scenario B, because the VOCs emitted from the individual sources were subtracted one by one. In this approach, the differences in simulated O_3 between scenario A and scenario B were the contributions of individual VOC sources to the local O_3 production.

Text S3. Uncertainties in HONO concentrations and the subsequent uncertainties in the contributions of HONO to OH formation and loss rates.

To evaluate the uncertainties of adopting the HONO concentrations in 2011 in the model, we calculated the average diurnal cycles of HONO in the 2007, 2013 and 2016 sampling campaigns (Figure S5), according to the diurnal patterns of HONO/NO_x ratios determined at the same site (Xu et al., 2015) and the in-situ measurements of NO_x. It was found that by adopting the values in 2011, the HONO concentrations were underestimated by 14.9% and 11.6% in 2007 and 2013, respectively, but were overestimated by 10.4% 2016. Further, the sensitivity tests indicated that the maximum underestimation (overestimation) of the total OH

production rate was 2.3±2.3% (21.6±5.2%) in 2007, 5.8±1.3% (3.4±1.0%) in 2013 and 5.7±1.3% (3.4±0.9%) in 2016. It should be noted that the maximum overestimation of the total OH production rate in 2007 (21.6±5.2%) occurred at 07:00 LT when the OH recycling was weak. During 08:00 – 19:00 LT, both the underestimation and overestimation of the simulated total OH production rates were less than 3%. Therefore, it was concluded that the simulated OH formation and loss rates were not largely biased by adopting the measured HONO at TC in 2011 in all the simulations.

Besides, the HONO concentrations calculated from the HONO/NO_x ratios and NO_x concentrations also had certain uncertainties. Thus, we did not use the calculated HONO concentrations to constrain the model. In fact, the consistent input of the diurnal cycle of HONO concentrations in the three sampling campaigns enabled us to look into the changes of O_3 and radical photochemistry induced by the other factors, such as VOCs, NO_x and meteorological conditions.

Table S1. Summary of the representative studies regarding O_3 pollution in Hong Kong.

Reference	Site	Measurement period	Nature of monitoring	Target	Main conclusions
Cheng et al, 2010	Wanqingsha (WQS), Guangdong and Tung Chung (TC), Hong Kong (HK)	Oct-Dec 2007	Suburban	O_3	O_3 formation was limited by VOCs at both sites. Carbonyls played important roles in photochemistry.
Cheng et al, 2013	TC, HK	Sep 2007 and Sep 2008	Suburban	O_3, VOCs	Major sources of VOCs in HK included consumer products, paint and printing solvent, road transport, and industrial, commercial, domestic and off-road transport.
Ding et al, 2004	Pearl River Delta (PRD)	Sep 2001	Large area	O_3	O_3 pollution events in PRD were closely associated with sea-land breezes and tropical cyclones.
Guo et al, 2011	WQS and TC	Oct-Dec 2007	Suburban	VOCs	Solvent use, vehicular emissions, biomass burning, LPG usage and gasoline evaporation dominated the sources of VOCs in PRD.
Guo et al, 2013a	Tsuen Wan (TW) and Tai Mao Shan (TMS), HK	Sep-Nov 2010	TW: Urban TMS: Mountainous	O_3	Less NO titration, vertical transport, valley breeze and regional transport caused higher O_3 at the mountainous site.
Huang et al, 2005	HK	1999-2003	Large area	O_3	Tropical cyclones, continental anticyclones and troughs were conducive to O_3 pollution events in HK.
Lam et al, 2005	TC, HK	Aug 1999	Suburban	O_3, VOCs	Local thermal circulation under calm synoptic conditions trapped air pollutants, resulting in O_3 enhancement in HK.
Ling et al, 2013	TC, HK	Sep-Nov 2010	Suburban	O_3	High O_3 in HK was a combined effect of both local formation and regional transport.
Ling et al, 2014	TW and TMS, HK	Sep-Nov 2010	TW: Urban TMS: Mountainous	O_3	Different O_3 production and destruction pathways at two sites. More aged air masses at the mountainous site favored O_3 formation.
Lyu et al, 2016a	Multiple, HK	Sep 2013 and Sep 2014	Urban Suburban Rural	VOCs	VOCs emitted from LPG-fueled vehicles significantly decreased at urban roadside sites. O_3 formation was limited by VOCs regardless of locations, while VOCs and NO_x co-limited O_3 formation in rural areas.
Lyu et al, 2016b	Mong Kok (MK), HK	Jun 2011-May 2014	Roadside	O_3, VOCs	Replacing catalytic converters in LPG-fueled vehicles led to substantial reductions of VOCs and NO_x emissions.
Lyu et al, 2017a	TC, HK	2005-2013	Suburban	VOCs	VOCs emitted from solvent usage and diesel exhaust decreased in HK from 2005 to 2013.

Ou et al, 2015	TC, HK	2005-2013	Suburban	VOCs	Vehicular exhaust, gasoline evaporation and LPG usage, consumer product and printing, architectural paints, and biogenic emissions were identified as the sources of VOCs in the study area.
So and Wang, 2003	Multiple, HK	Jun 1999-May 2000	Urban Suburban Rural	O_3	Air quality in rural areas was frequently influenced by regional air masses, and was predominantly affected by local emissions in urban areas.
Wang et al, 2017a	TC, HK	2005-2014	Suburban	O_3	Locally produced autumn O_3 decreased in HK, which was reversed by regionally-transported O_3 between 2005 and 2013.
Wang et al, 2018a	Wan Shan Island (WSI), GD	Aug-Nov 2013	Rural	O_3	O_3 formation switched from the NO_x-limited regime on low O_3 days to VOC-limited regime on high O_3 days over South China Sea.
Xu et al, 2008	Linan, Zhejiang	Aug 1991-Jul 2006	Rural	O_3	Monthly highest 5% of O_3 increased from 1991 to 2006, with enhanced variability, likely due to the increased NO_x emissions.
Xue et al, 2014a	TC, HK	Sep-Nov of 2002-2013	Suburban	O_3	Increase of regionally-transported O_3 offset the decrease of locally-produced O_3 and resulted in the increase of observed O_3 in the autumn in HK during 2002-2013.
Zhang et al, 2007	Multiple, HK	Oct-Dec 2002	Urban Suburban Rural	O_3	50-100% of O_3 enhancement during O_3 episodes in HK was explained by local photochemical formation, following the oxidation of anthropogenic VOCs.

Table S1. Summary of the sampling periods, VOC sampling dates and number of samples in the 2007, 2013 and 2016 sampling campaigns.

Year	Sampling period	Month	Date	Number of NMHC samples	Number of OVOC samples
2007	23 Oct.–1 Dec.	Oct.	26-27	96	28
		Nov.	13, 15-17, 23		
		Dec.	1		
2013	11 Aug.–22 Nov.	Sept.	11-12, 26	146	124
		Oct.	2-4, 9-10, 17, 22-25, 30-31		
		Nov.	15, 19-21		
2016	25 Sept. – 29 Nov.	Sept.	26	172	123
		Oct.	14-17, 23, 31		
		Nov.	1-7,14-18		
Total				414	275

Table S3. Instruments, analysis techniques, detection limits and time resolutions for the real-time measurements of trace gases at the TC air quality monitoring station.

Species	Instrument	Analysis technique	Detection limit	Time resolution
SO_2	API 100E	UV fluorescence	0.4 ppb	1 sec
CO	API 300	Non-dispersive infra-red absorption with gas filter correlation	<0.050 ppm	1 sec
NO-NO_2-NO_x	API 200A	Chemiluminescence	0.4 ppb	1 sec
O_3	API 400	UV absorption	0.6 ppb	1 sec

Table S4. Summary of limits of detection (LoDs), precisions and accuracies of the GC-MSD/FID/ECD systems used for NMHCs analyses of whole air samples collected in 2007, 2013 and 2016 (Simpson et al., 2010; Wang et al., 2018).

Institution	Year	Limit of Detection	Precision	Accuracy
UCI	2007	3-10 pptv	3%	5%
GIG	2013	3-57 pptv	2-5%	5%
HKPolyU	2016	3-10 pptv	5%	5%

Table S5. Statistics of VOC mixing ratios measured in 2007, 2013 and 2016. The 95% C.I., Max. and S.D. denote the 95% confidence interval, maximum and standard deviation of the mixing ratios of VOC species, respectively (Unit: pptv).

VOC species	2007			2013			2016		
	Mean±95%CI	Max.	S.D.	Mean±95%CI	Max.	S.D.	Mean±95%CI	Max.	S.D.
Ethane	1587.6±37.3	1994.6	186.7	1918.9±140.1	5700.4	1123.4	1729.1±85.3	3951.2	655.6
Ethene	1388.7±53.5	2284.7	267.3	1074.9±94.3	4529.8	751.9	886.8±79.1	4335.5	605.3
Ethyne	1939.3±105.3	3855.4	526.3	1563.4±94.8	3339.0	760.0	1399.2±83.1	4254.7	637.5
Propane	2826.2±94.1	3889.6	472.0	1619.1±110.4	5826.3	883.4	2308.4±224.2	13269.8	1715.9
Propene	325.2±34.0	1036.7	169.9	296.1±20.3	1052.3	162.7	192.3±13.8	773.6	105.5
i-Butane	790.9±40.7	1269.3	203.6	1556.4±115.5	5778.5	922.7	901.5±67.5	3229.9	516.6
n-Butane	1562.4±124.3	3360.3	621.5	1402.6±95.8	5353.7	767.8	1403.8±116.3	5001.2	893.8
1-/i-Butene	275.1±71.2	2945.2	356.1	240.7±70.6	5944.6	566.2	98.0±9.4	715.8	71.7
trans-2-Butene	22.5±6.0	213.4	29.7	31.2±6.7	387.1	42.5	12.1±2.9	184.1	18.3
cis-2-Butene	24.4±6.0	201.9	29.7	25.2±5.0	275.2	32.4	9.3±2.8	178.5	17.5
3-methyl-1-Butene	12.0±2.4	76.6	11.9	35.6±16.0	332.0	67.2	8.7±5.5	207.0	26.6

2-methyl-1-Butene	16.4 ±3.3	89.0	16.3	47.4 ±25.3	1074.0	146.6	17.4 ±11.4	765.6	73.4
cis-2-Pentene	28.6 ±5.1	130.4	25.4	34.5 ±7.9	273.9	46.8	5.5 ±3.4	130.1	16.4
2-methyl-2-Butene	4.6 ±1.0	25.8	4.8	37.4 ±14.6	558.0	84.3	10.2 ±3.6	139.3	17.5
Butyne	41.0 ±6.3	171.2	31.5	40.5 ±12.1	406.7	58.6	18.5 ±2.8	142.2	18.5
i-Pentane	1809.6 ±339.6	7793.6	1697.8	827.5 ±63.3	4646.9	504.0	466.3 ±33.2	1681.2	254.1
n-Pentane	351.9 ±63.7	2271.2	318.7	50.1 ±8.6	416.2	59.9	265.1 ±25.1	1104.0	192.5
1-Pentene	20.4 ±5.7	244.3	28.2	50.1 ±8.6	416.2	59.9	15.6 ±2.9	182.5	20.3
trans-2-Pentene	15.3 ±4.1	182.0	20.8	23.6 ±7.7	302.1	41.4	9.8 ±4.9	189.6	24.1
2-Methylpentane	268.8 ±68.7	2253.0	343.6	257.1 ±29.6	1643.9	237.9	195.5 ±27.1	1171.6	204.9
n-Hexane	1785.2 ±547.3	17974.4	2736.1	930.6 ±147.7	9829.0	1182.2	163.4 ±23.8	1426.7	182.1
n-Heptane	113.8 ±39.3	1196.3	196.7	100.2 ±12.8	877.3	102.4	65.9 ±5.8	290.7	44.7
n-Octane	42.4 ±9.6	245.2	48.1	47.5 ±8.9	739.3	70.4	34.0 ±3.9	188.0	30.4
2,2-Dimethylbutane	18.7 ±2.2	64.8	11.3	52.7 ±8.7	719.6	65.0	20.2 ±2.0	91.9	14.2
2,3-	31.2 ±17.1	822.5	84.5	68.8 ±7.1	389.3	55.9	46.3 ±7.3	311.9	50.0

Dimethylbutane									
3-Methylpentane	1911.5 ±423.0	10292.0	2114.7	172.0 ±20.5	1260.3	164.4	131.8 ±18.9	1025.8	144.7
Cyclohexane	66.1 ±29.1	905.4	145.7	84.1 ±8.7	601.5	70.3	68.1 ±8.0	414.4	54.3
2-Methylhexane	49.0 ±16.4	557.0	82.1	85.7 ±9.7	429.6	77.5	205.8 ±19.2	492.8	89.9
3-Methylhexane	172.8 ±53.5	1651.2	266.3	171.5 ±19.4	1171.5	155.6	43.7 ±5.4	271.3	37.0
n-Nonane	29.1 ±6.4	226.8	32.2	47.6 ±8.1	621.6	64.4	39.9 ±7.3	477.2	56.4
n-Decane	457.3 ±138.9	3680.5	694.4	72.2 ±15.7	1198.3	126.3	34.0 ±3.9	188.0	30.4
n-Undecane	71.9 ±13.6	319.7	65.9	90.8 ±18.1	1367.5	145.4	--	--	--
Isoprene	270.6 ±53.0	868.5	264.9	417.0 ±44.4	1561.0	343.4	409.1 ±52.5	3122.0	402.0
α-Pinene	261.8 ±191.5	6810.0	957.3	29.9 ±4.4	321.5	34.2	21.1 ±2.9	218.0	22.2
β-Pinene	30.3 ±10.1	306.4	50.6	53.8 ±7.3	314.5	57.5	9.9 ±0.7	32.0	5.4
Benzene	567.0 ±99.7	3761.2	498.5	493.1 ±33.2	2308.0	266.3	257.3 ±14.5	658.2	110.3
Toluene	2878.9 ±845.3	26556.8	4225.8	1445.3 ±149.2	6494.2	1196.5	1169.5 ±229.5	13376.0	1601.8
Ethylbenzene	358.8 ±63.2	1597.7	316.3	389.1 ±52.3	4274.0	419.5	193.6 ±20.7	1350.2	159.1

m/p-Xylene	411.1 ±82.1	1789.7	410.7	491.8 ±109.7	10168.0	879.8	299.4 ±28.4	1600.8	217.9
o-Xylene	168.1 ±30.0	773.5	150.3	231.3 ±34.1	2082.0	274.1	151.7 ±13.7	891.2	105.0
1,3,5-Trimethylbenzene	43.8 ±8.8	323.5	44.3	38.6 ±8.4	680.3	67.5	11.6 ±1.6	125.5	12.7
1,2,4-Trimethylbenzene	177.3 ±40.1	1527.5	200.6	143.3 ±25.1	1492.3	201.7	39.6 ±5.6	336.7	42.9
1,2,3-Trimethylbenzene	64.7 ±23.8	940.9	117.8	63.1 ±11.6	809.7	93.4	16.7 ±3.5	320.3	27.2
i-Propylbenzene	7.4 ±1.2	38.0	6.3	16.5 ±1.8	111.1	14.2	7.5 ±0.7	63.0	5.8
n-Propylbenzene	16.4 ±2.6	68.9	13.0	34.3 ±4.3	305.2	34.5	12.4 ±2.0	188.6	15.3
3-Ethyltoluene	34.6 ±7.2	212.4	36.1	74.0 ±10.6	653.0	85.5	24.7 ±2.9	171.4	22.4
4-Ethyltoluene	18.1 ±3.4	114.4	17.1	45.4 ±6.1	429.8	48.7	16.6 ±2.4	220.2	18.3
2-Ethyltoluene	23.2 ±4.3	143.0	21.5	40.4 ±6.7	476.3	53.9	14.0 ±2.1	186.1	16.3
Formaldehyde	8608.3 ±1298.0	30244.3	6352.3	2729.0 ±146.5	6403.5	1123.8	2673.3 ±283.1	13633.0	2171.5
Acetaldehyde	9853.8 ±1732.6	46380.0	8198.0	1395.9 ±81.1	3694.8	622.2	779.4 ±92.1	3126.0	649.4
Acetone	12786.4 ±2712.9	75590.0	13131.5	5156.2 ±421.3	22921.5	3231.7	4995.6 ±460.6	13370.9	3469.7

Propionaldehyde	--	--	--	325.0 ± 38.2	1593.2	247.0	1547.9 ± 547.2	3071.6	1081.3

Table S6. Comparison of meteorological conditions in the autumns of 2007, 2013 and 2016 (HKO, 2017).

	2007		2013		2016	
	Mean ± 95%C.I.	Max.	Mean ± 95%C.I.	Max.	Mean ± 95%C.I.	Max.
Temperature (℃)	23.5±0.4	30.0	25.2±0.3	33.9	25.0±0.3	32.7
Relative humidity (%)	64.4±1.4	80.0	58.6±1.3	83.1	77.1±0.7	94.5
Solar radiation (W m^{-2})	190.3±37.7	788.9	159.2±21.3	869.1	119.8±18.2	829.3
Pressure (hPa)	1016.9±0.4	1024.3	1015.0±0.3	1023.1	1012.3±0.3	1020.2
Wind speed at the sampling site (m s^{-1})	2.3±0.2	5.3	1.0±0.1	3.2	0.9±0.1	4.3
Wind speed at HKIA* (m s^{-1})	4.7±0.3	10.8	4.8±0.4	11.7	4.5±0.3	12.4

*HKIA: Hong Kong International Airport.

Table S7. Number of O_3 episode days identified under the tropical cyclone, continental anticyclone and low pressure trough in the autumns of 2007, 2013 and 2016.

Year	Total No. of Episode	Tropical cyclone	Continental anti-cyclone	Low Pressure trough
2007	15*	8 (4 typhoons)	8	1
2013	16	11 (5 typhoons)	5	0
2016	5	4 (3 typhoons)	0	1

*Two O_3 episode days were under the combined influence of tropical cyclone and continental anticyclone.

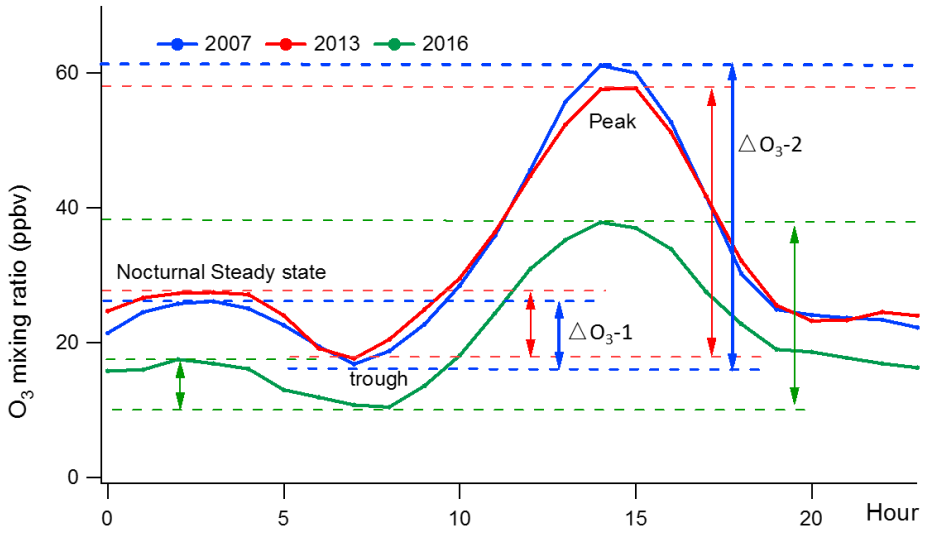

Figure S1. Average diurnal cycles of O_3 in the 2007, 2013 and 2016 sampling campaigns. ΔO_3-1: O_3 decrease in the early morning driven by NO titration; ΔO_3-2: photochemically formed O_3 in the daytime (diurnal cycle of O_3 in 2007 as an example).

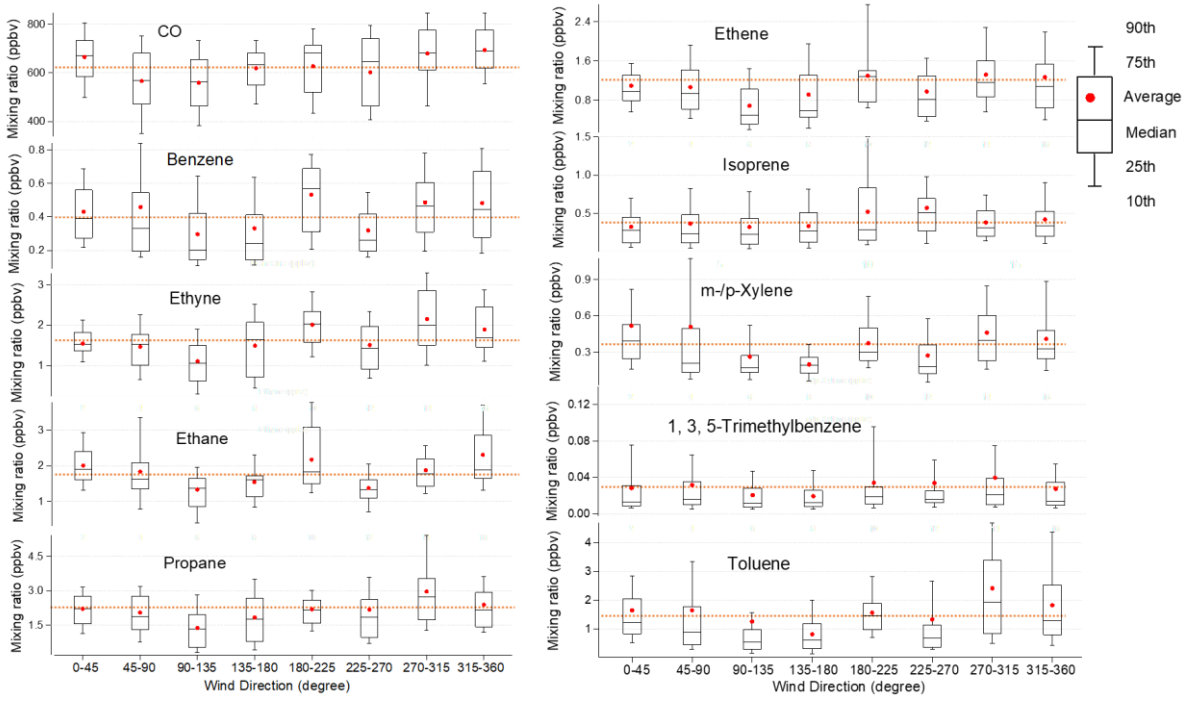

Figure S2. Average mixing ratios of some O_3 precursors in different wind sectors at TC in the three sampling campaigns. The orange dotted lines represent average concentrations under light winds (wind speed < 2 m/s).

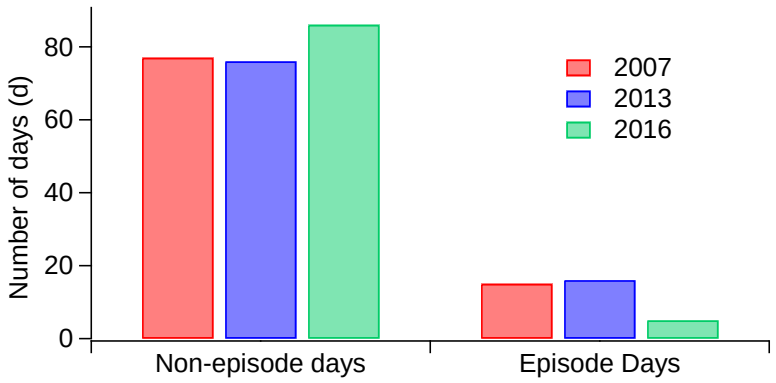

Figure S3. Number of O_3 episode days and non-O_3 episode days in the autumns of 2007, 2013 and 2016.

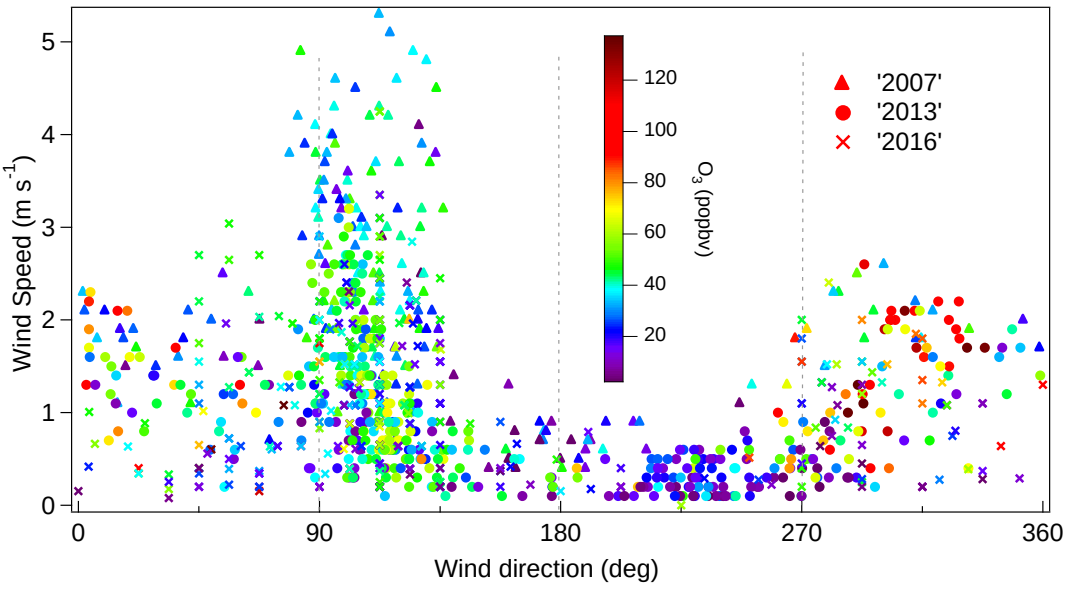

Figure S4. Relationship between the hourly observed O_3 and the wind fields at TC in the three sampling campaigns.

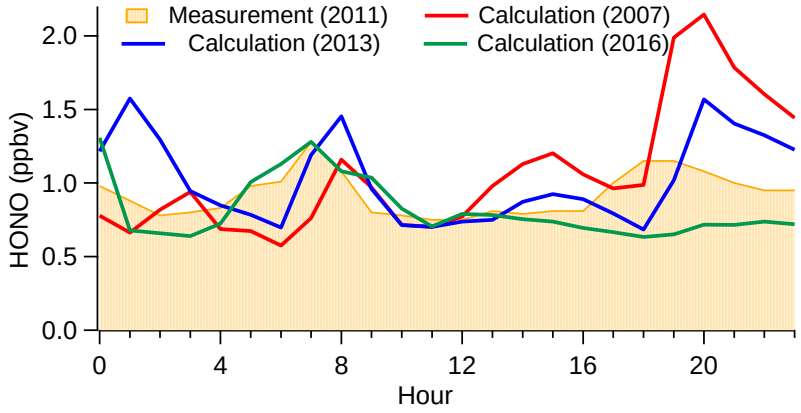

Figure S5. Diurnal cycles of HONO mixing ratios measured at TC in the autumn of 2011 and those calculated from the measured HONO/NO_x ratios and NO_x mixing ratios at the same site in the three sampling campaigns.

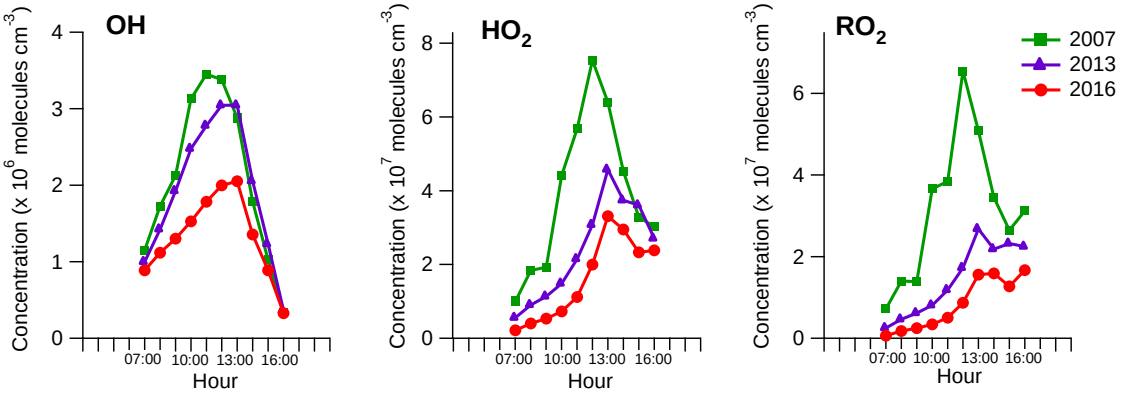

Figure S6. Average diurnal profiles of the simulated OH, HO_2 and RO_2 concentrations on VOC sampling days in 2007, 2013 and 2016. The rebounding of HO_2 and RO_2 concentrations in the late afternoon in 2007 and 2016 was caused by the substantial increases in the concentrations of some VOCs or OVOCs in several samples.

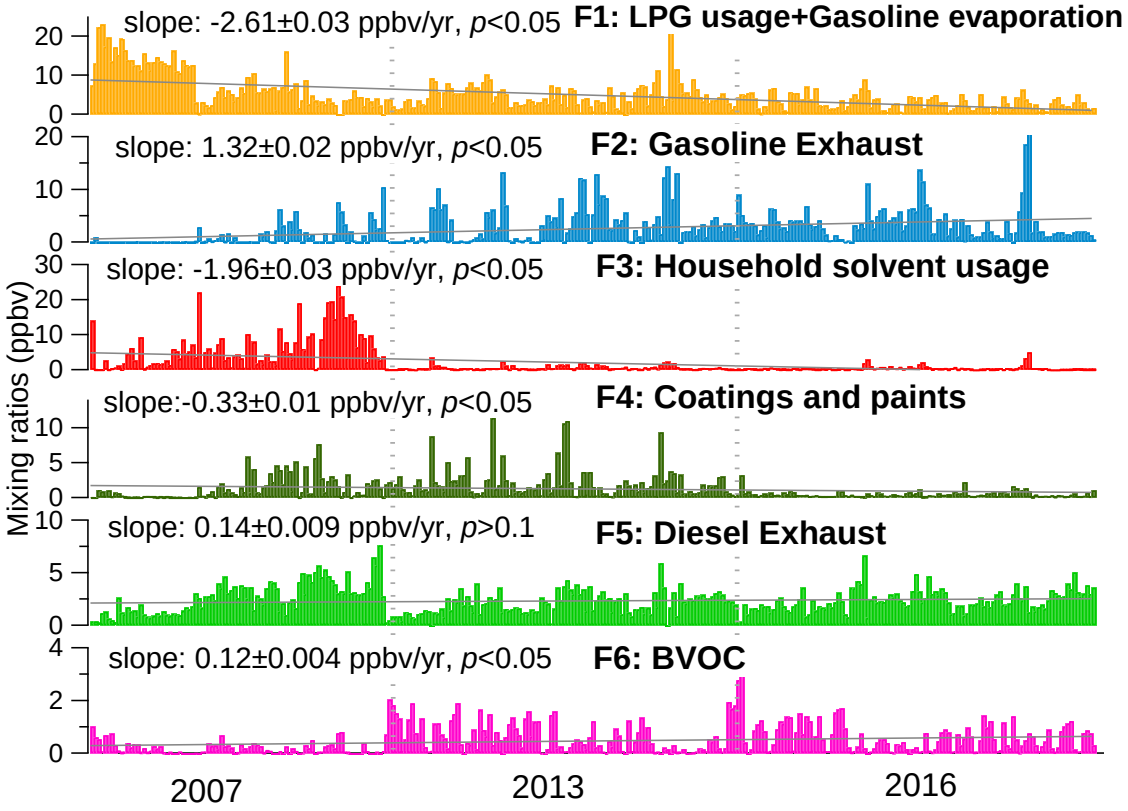

Figure S7. Total mixing ratio of VOCs emitted from each individual source extracted from PMF in the 2007, 2013 and 2016 sampling campaigns. The solid lines represent the linear regressions of the VOC mixing ratios against the sequence number of the samples, with the slope being converted to yearly rates.

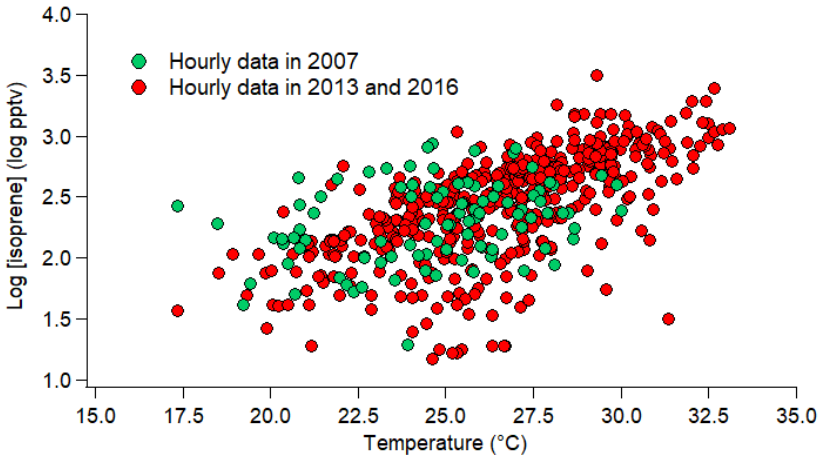

Figure S8. Relationship between the common logarithm of isoprene mixing ratios and temperature.